Atmospheric Environment 250 (2021) 118265

Contents lists available at ScienceDirect

Atmospheric Environment

journal homepage: http://www.elsevier.com/locate/atmosenv

VIIRS Environmental Data Record and Deep Blue aerosol products: validation, comparison, and spatiotemporal variations from 2013 to 2018 in China

Lijie He [a], Lunche Wang [b,**], Zhengqiang Li [c], Daoyang Jiang [b], Lin Sun [d], Dong Liu [e], Lei Liu [f], Rui Yao [b], Zhigao Zhou [g], Jing Wei [h,*]

[a] College of Public Administration, Huazhong Agricultural University, Wuhan, China
[b] School of Geography and Information Engineering, China University of Geosciences, Wuhan, China
[c] State Environmental Protection Key Laboratory of Satellite Remote Sensing, Aerospace Information Research Institute, Chinese Academy of Sciences, Beijing, China
[d] College of Geodesy and Geomatics, Shandong University of Science and Technology, Qingdao, China
[e] State Key Laboratory of Modern Optical Instrumentation, College of Optical Science and Engineering, International Research Center for Advanced Photonics, Zhejiang University, Hangzhou, China
[f] College of Earth and Environmental Sciences, Lanzhou University, Lanzhou, China
[g] School of Resource and Environmental Science, Wuhan University, Wuhan, China
[h] Department of Atmospheric and Oceanic Science, Earth System Science Interdisciplinary Center, University of Maryland, College Park, MD, USA

HIGHLIGHTS

- VIIRS EDR and DB AOD products are validated and compared in China.
- Both two products are significantly refined after quality assurance control.
- VIIRS DB retrievals are more accurate with smaller uncertainties than EDR retrievals.
- AOD has significantly decreased by 0.0008 per year in China from 2013 to 2018.

ABSTRACT

Recently, the Deep Blue (DB) algorithm has been successfully applied to the Visible Infrared Imaging Radiometer Suite (VIIRS) to expend the long-term aerosol records over land in conjunction with the Environmental Data Record (EDR) product. However, the overall accuracy and uncertainty of VIIRS DB and EDR Aerosol Optical Depth (AOD) products are still unclear in China, in particular, due to the sparse distribution of ground observation stations. Therefore, the objective of this study is to evaluate and compare VIIRS EDR and DB AOD retrievals against ground measurements collected from both Aerosol Robotic Network (AERONET) and Chinese Sun-sky radiometer Observation Network (SONET) in China from 2013 to 2018. Results suggest that both EDR and DB products have a significant refinement after quality assurance (QA) controlling. DB (QA = Best) performs best with high correction (R = 0.92), and up to 80.32% of AOD matches falling within the expected error (EE), while approximately 46% of EDR (QA = Best) AOD retrievals are overestimated. However, EDR has a higher retrieval frequency than DB over most regions of China, except for the arid and semi-arid areas such as the Northwest. Generally, despite some exceptions, both EDR and DB products perform relatively poorly in summer for all statistics. Furthermore, the error analysis explains that DB is less sensitive to varying air pollution levels, diverse aerosol types, and different surface conditions, while the pattern of EDR is complicated. In addition, due to the common algorithmic heritage, both VIIRS EDR and MODIS DT products only show good matching over dark surfaces, while VIIRS DB and MODIS DB algorithms have good performance over both dark and bright surfaces. Finally, both EDR and DB products have shown significant downward AOD trends equal to −0.0008 per year ($p < 0.01$) in China during the last past six years, especially for three typical urban agglomerations. These evaluation results are expected to provide appropriate guidance for the application of VIIRS aerosol products in China.

* Corresponding author.
** Corresponding author.
E-mail addresses: wang@cug.edu.cn (L. Wang), weijing_rs@163.com (J. Wei).

https://doi.org/10.1016/j.atmosenv.2021.118265
Received 7 October 2020; Received in revised form 23 January 2021; Accepted 8 February 2021
Available online 13 February 2021

1. Introduction

Aerosols are solid and liquid particles suspended in the atmosphere, which have significant effects on global climate changes, directly by scattering or absorbing solar shortwave radiation and indirectly by modifying cloud properties (Sundström et al., 2015; Wei et al., 2019a; Xia et al., 2016; He et al., 2017, 2020). To better understand the impacts of aerosols, long-term aerosol data records with high accuracy are needed (Wei et al., 2021a,b). Satellite remote sensing enables us to obtain aerosol information on a large scale (Popp et al., 2016; Martins et al., 2017; Mei et al., 2019a). Moderate Resolution Imaging Spectroradiometer (MODIS) onboard Terra and Aqua satellites is one of the most popular sensors to retrieve global aerosol optical properties based on Dark Target (DT) algorithm over vegetated land and ocean (Levy et al., 2013), and Deep Blue (DB) algorithm over land only (Hsu et al., 2013). The MODIS aerosol products have been updated to the latest Collection 6.1 (C6.1) with a series of improvements in quality assurance, heavy smoke detection, and surface modeling for elevated terrain, which has been proved to be more accurate than previous collections (Hsu et al., 2013; Sayer et al., 2014; Gupta et al., 2016; Mei et al., 2019b; Wei et al., 2019a). However, since MODIS has been operationally running for more than approximately two decades, there is an urgent need to expend the long-term continuous aerosol data records for climate researches. Therefore, in late 2011, the Suomi National Polar-orbiting Partnership (S-NPP) Visible Infrared Imaging Radiometer Suite (VIIRS) was successfully launched and is expected to inherit MODIS to continue the Earth Observing System observation in the future (Cao et al., 2013; Liu et al., 2014).

Originally, the National Oceanic and Atmospheric Administration (NOAA) has generated the VIIRS Environmental Data Record (EDR) Level 2 aerosol products using a refined algorithm similar to the MODIS DT algorithm (Jackson et al., 2013; Wei et al., 2019b), which is publicly available on May 2, 2012. To date, the VIIRS EDR aerosol products have been widely validated and showed noticeable differences from local to global scales (Liu et al., 2014; Huang et al., 2016; Xiao et al., 2016; Zhu et al., 2017; He et al., 2018). Note that the EDR aerosol product cannot retrieve AOD over bright surfaces, in cloud-affected pixels, over inland water, or at night (DeLuccia et al., 2012; Jackson et al., 2013). For addressing the shortcoming, on February 6, 2018, the National Aeronautics and Space Administration (NASA) has released the VIIRS DB Level 2 aerosol product based on the second-generation DB algorithm over land and the Satellite Ocean Aerosol Retrieval (SOAR) algorithm over ocean (Hsu et al., 2019; Sayer et al., 2018, 2019). The initial DB algorithm retrieves aerosols based on the assumption that the surface reflectance (except for snow) at the blue spectral band (~412–490 nm) is comparatively darker than that of other bands over bright surfaces (Hsu et al., 2006). Then, the initial DB algorithm is able to retrieve AODs on the bright surface pixel-by-pixel by creating a surface reflectance data base from atmospherically corrected satellite observations and by using an assumed aerosol optical model (Hsu et al., 2006). Subsequently, in order to expand AOD retrieve coverages from bright surfaces to all snow-free land surfaces, a second-generation DB algorithm is developed to VIIRS (Hsu et al., 2013). This is achieved by developing new spectral-directional relationships for vegetated surface reflectance, similar in principle to the DT method but with additional stratification by scene Normalized Difference Vegetation Index (NDVI), geometry, and subcategories of cover type (e.g., croplands vs. forests) to give a bidirectional reflectance distribution function (BRDF) model (Hsu et al., 2013). Additional refinements are also made for the surface database creation, cloud screening, aerosol optical models, and quality assurance (QA) tests to address the limitations of the MODIS C6 DB algorithm (Hsu et al., 2019). However, to date, there has been little validation work on the VIIRS DB aerosol product, especially for local regions, such as China, where features severe air pollution with abundant anthropogenic aerosol emissions. In addition, there are few aerosol ground monitoring stations in China, which severely limits such work and increases the difficulties of the future algorithm improvement.

Table 1
Parameters of the Aqua-MODIS and NPP-VIIRS sensors.

Parameters	Aqua-MODIS	NPP-VIIRS
Orbit altitude	705 km	824 km
Swath Width	2330 km	3040 km
Equator crossing time (Local Time)	13:30	13:30
Sensor zenith angle range	±64°	±70°
Bands used for aerosol retrievals	0.412, 0.466, 0.646, 0.856 1.24, 2.11, 11, and 12 μm	0.412, 0.445, 0.488, 0.550, 0.555, 0.672, 0.746, 0.865, 1.240, 1.610, and 2.250 μm
Spatial resolution	250 m (bands 1–2) 500 m (bands 3–7) 1000 m (bands 8–36)	375m (Imagery Bands) 750m (Moderate Bands)
Global coverage	1–2 days	1 day
Repeat cycle	~16 days	~16 days

Therefore, in this study, we try to comprehensively compare the VIIRS EDR and DB AOD products against ground measurements from AERONET (Aerosol Robotic Network) and SONET (Sun-sky radiometer Observation Network) monitoring stations in China during 2013–2018. Section 2 briefly introduces VIIRS and in-situ AOD data as well as other auxiliary data. The evaluation approach and spatiotemporal analysis method are clarified in Section 3. Section 4 elaborates on the overall accuracy of the VIIRS EDR and DB AOD products from spatial and temporal perspectives using AERONET/SONET AOD observations. Section 5 presents the error analyses of EDR and DB algorithms to the diverse surface and varying atmospheric conditions. Section 6 compares VIIRS EDR and DB products with MODIS official aerosol products. Furthermore, since the long-term AOD trend in China has always been inconclusive (Zhang et al., 2017; He et al., 2018), section 7 also estimates the performance of the EDR and DB AOD products in retrieving long-term trend of AOD across China and illustrates the spatiotemporal variations of China's aerosols in the past six years. Finally, a brief summary is shown in Section 8. Such a systematic analysis of VIIRS aerosol products has not been previously reported in China and is expected to be useful for future climate change and air quality studies, as well as the development of aerosol algorithms.

2. Data source

2.1. VIIRS AOD products

VIIRS launched on Suomi-NPP satellite is a passive multispectral imaging radiometer with 22 spectral bands from visible to infrared spectrum (412–2250 nm). Suomi-NPP orbit has a similar equator crossing time (13:30) with Aqua MODIS. VIIRS has a broader swath width of 3040 km and a larger sensor zenith angle up to 70° than MODIS (~2330 km, 64°). Therefore, in surface and aerosol property assumptions, the uncertainties related to angles have greater impacts on the retrieval accuracy of the VIIRS aerosol product when compared to the MODIS product (Hsu et al., 2019). More details about the characteristics of MODIS and VIIRS instruments are shown in Table 1.

Nowadays, VIIRS has released two operational global-coverage daily aerosol Level 2 products at the same spatial resolution of 6 km, including the NOAA EDR and NASA DB AOD products. The VIIRS EDR land aerosol algorithm is applied to dark surfaces and is the heritage of the MODIS DT land algorithm (Liu et al., 2014). Both algorithms retrieve AOD from the reference channels for the candidate aerosol models (or mixtures) and select the optimal AOD by finding the minimum residuals between the calculated and the prescribed surface reflectance ratios. However, the VIIRS EDR and MODIS DT land aerosol algorithms are structurally

Table 2
Comparison between MODIS DB and VIIRS DB aerosol products.

	MODIS DB	VIIRS DB	VIIRS DB Refinement
Product resolution	10×10 km^2	6×6 km^2	Imporve the spatial resolution of AOD
Spatial coverage	Land only	Land and ocean	Extend the spatial coverage of AOD
Improved smoke mask	No	Yes	Distinguish the smoke plumes from urban/industrial aerosols
Improved dust aerosol optical models	No	Yes	Retrieve continuous AOD in the Saharan dust plume
Improved in surface determining scheme	No	Yes	Retrieve better AOD over vegetated surfaces

different. The VIIRS EDR land aerosol algorithm dynamically selects a single model from five candidate aerosol models (dust, low absorption smoke, high absorption smoke, clean urban, and polluted urban). This differs from the MODIS DT land algorithm, which assigns two aerosol models based on location and season but allows the retrieval to mix these two models (Jackson et al., 2013; Liu et al., 2014). The EDR aerosol product is the Level 2 product. It is retrieved by the VIIRS EDR land algorithm and created from the intermediate product (IP) product through a system of quality checks, data filtering, and spatial aggregation. Note that the current EDR product has no aerosol retrievals over special pixels such as bright surfaces, inland water, and cloud-contaminated areas. In addition, the AOD value of EDR product is limited to the range of 0.0–2.0, limiting in capturing the severe polluted events with high aerosol loadings (DeLuccia et al., 2012).

The initial DB algorithm retrieves aerosols over bright land surfaces (such as deserts, bare soil, and urban areas) based on the assumption that the surface reflectance at the deep blue band is far smaller than that of other bands over bright surfaces (Hsu et al., 2006). Then, a second-generation DB algorithm extends aerosol retrievals from darkest surfaces to brightest surfaces, covering all cloud- and snow-free land surfaces (Hsu et al., 2013). The DB algorithm has been applied to the MODIS and VIIRS aerosol products (Hsu et al., 2019; Sayer et al., 2018, 2019). However, several major refinements have been made in the VIIRS DB algorithm compared to MODIS C6 DB (Table 2). For example, the retrieval coverage of DB is only available over land for MODIS, while for VIIRS, it extends to both land and ocean for VIIRS by combining with the SOAR algorithm (Sayer et al., 2018). In addition, the VIIRS DB algorithm has developed a new smoke mask using spectral curvature of the reflectance at the top of the atmosphere to distinguish the smoke plumes from urban/industrial aerosols. As a result, by combining the smoke mask with AOD and Ångström exponent (AE), a new aerosol-type product is produced to the VIIRS DB aerosol data suite, which is classified by dust, urban/industrial, smoke, high-altitude smoke, mixed, and background aerosols (Hsu et al., 2019). Besides, consistent dust models are improved in VIIRS DB aerosol retrievals for solving the problem that MODIS DB cannot continuously retrieve AOD in the Sahara dust plume. Furthermore, the VIIRS DB algorithm retrieves AOD by employing the short-wave infrared (SWIR) and near infrared (NIR) channels for different vegetated surfaces (Hsu et al., 2019). Different from the MODIS C6, many refinements made in the VIIRS DB algorithm have also been implemented in the MODIS C6.1. However, due to different data processing schedules, the MODIS C6.1 DB algorithm lacks some enhancements to the VIIRS DB algorithm, e.g., the use of the NIR channel for cropland and the

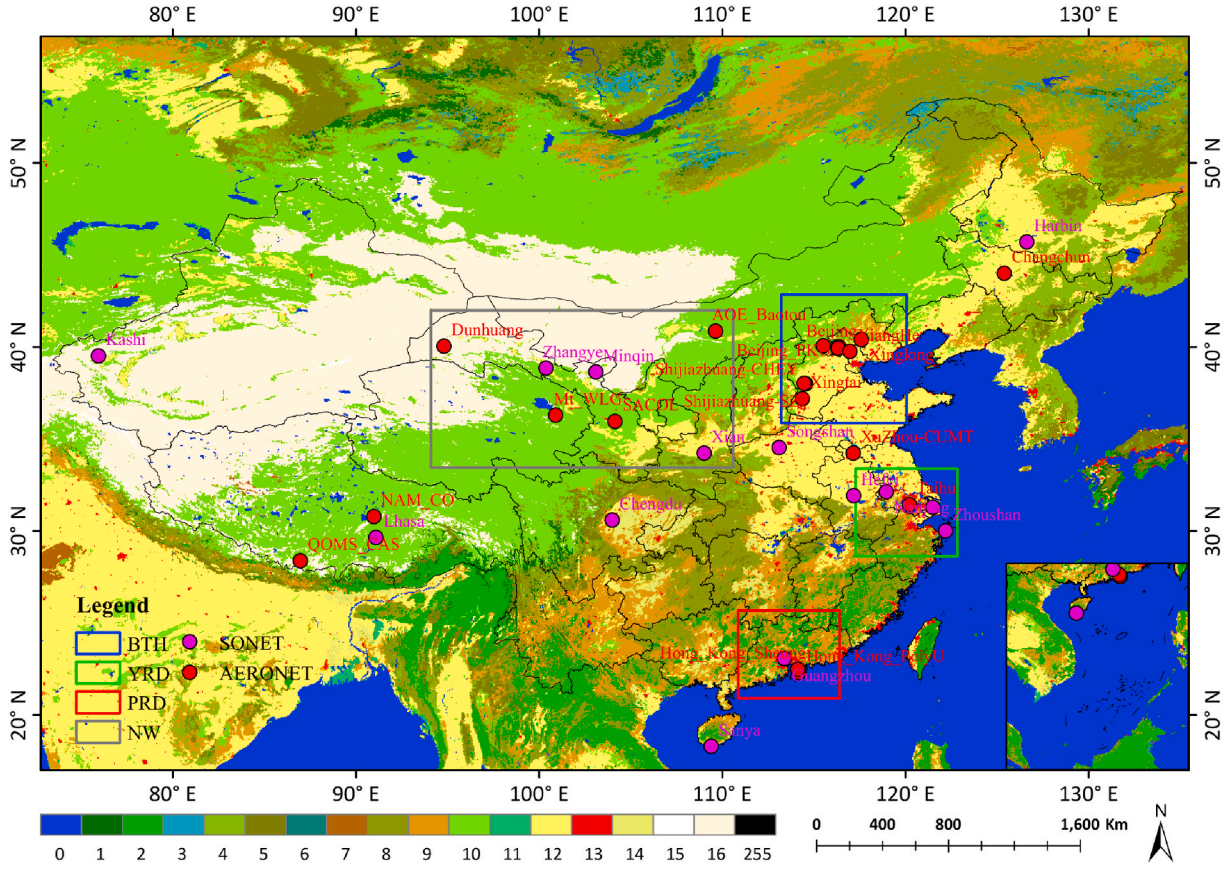

Fig. 1. Spatial distribution of AERONET (marked as red dots) and SONET (marked as pink dots) ground monitoring stations in China, where BTH, YRD, PRD, and NW represent the Beijing-Tianjin-Hebei, the Yangtze River Basin, the Pearl River Basin, and the Northwest region (NW), respectively. The background image refers to the land use type obtained from the MCD12C1 product. (For interpretation of the references to color in this figure legend, the reader is referred to the Web version of this article.)

improvement of nonspherical dust models; and it does not extend the upper limit of retrieved AOD from 3.5 to 5.0 (Sayer et al., 2019). Further algorithm information can be found at https://deepblue.gsfc.nasa.gov.

For both VIIRS Level 2 EDR and DB AOD products, Quality Assurance (QA) is provided to donate different data-quality levels of AOD retrievals based on a series of individual tests (Wei et al., 2018). In this study, the daily VIIRS EDR and DB AOD products with all (QA = All) and the best (QA = Best) quality in China from 2013 to 2018 are employed.

2.2. Ground-based AOD measurements

AERONET provides aerosol optical and microphysical properties every 15 min at a wide spectral range from visible to NIR channels (Holben et al., 1998; Giles et al., 2019; Sayer 2020). The AOD observations have a low systemic bias of ~0.01–0.02 and are classified into three quality levels, i.e., Level 1.0 (unscreened), Level 1.5 (cloud screened), and Level 2.0 (cloud screened and quality assured). In this study, AERONET Version 3 Level 2.0 and Level 1.5 instantaneous AOD and AE observations at 22 monitoring stations in China from 2013 to 2018 are collected (Fig. 1).

Besides the widely used AERONET network, the SONET network is also included to provide additional ground observation stations uniformly covered the whole of China. SONET is a ground-based aerosol network organized by the Chinese Academy of Science, which mainly provides aerosol properties at visible and near-infrared wavelengths in China. The SONET AOD observations also have a low systemic bias of ~0.25%–0.5% and undergone cloud screening and quality assurance followed AERONET protocols (Li et al., 2018). Here, SONET Level 1.5 AOD and AE observations at 14 monitoring stations are collected (Fig. 1). Table 3 shows detailed information about the aerosol monitoring stations in China.

2.3. Auxiliary data

For in-depth analysis, some auxiliary data, including the MODIS monthly NDVI and annual land-use type products at a spatial resolution of approximately 5 km, as well as the landform type at 1 km resolution, are also collected. For comparison purposes, the latest Aqua MODIS C6.1 DT and DB aerosol products at a coarser spatial resolution of 10 km in China covering the same period are collected, and only the best-quality AOD retrievals (QA = Best) are used here. Table 4 summarizes the data sources used in our study.

Table 4
Summary of satellite remote sensing and ground measured data set used in our study.

Product	Content	Spatial resolution	Temporal resolution	Time period
VAOOO	EDR AOD (QA = All)	6 km	Daily (Swath)	2013–2018
	EDR AOD (QA = Best)	6 km	Daily (Swath)	2013–2018
AERDB	DB AOD (QA = All)	6 km	Daily (Swath)	2013–2018
	DB AOD (QA = Best)	6 km	Daily (Swath)	2013–2018
AERONET	AOD	In situ	15 min/ Monthly	2013–2018
	$AE_{440nm-675nm}$	In situ	15 min	2013–2018
MYD13C2	NDVI	0.05°	Monthly	2013–2018
MCD12C1	Land use type	0.05°	Yearly	2013–2018
Topography	Landform type	1 km	–	2009
MYD04_L2	DT AOD (QA = Best)	10 km	Daily (Swath)	2013–2018
	DB AOD (QA = Best)	10 km	Daily (Swath)	2013–2018

Table 3
Detailed information on used aerosol ground monitoring stations across China.

No.	Site name	Longitude	Latitude	Altitude	Land use type	Topography
1	Songshan	113.0961	34.5348	475	Forest	Mountian
2	Xinglong	117.578	40.396	970		Mountian
3	AOE_Baotou	109.629	40.852	1270	Grassland	Plateau
4	Hong_Kong_Sheung	114.117	22.483	40		Mountian
5	Lingshan_Mountain	115.496	40.054	1653		Mountian
6	Mt_WLG	100.896	36.283	3816		Mountian
7	NAM_CO	90.962	30.773	4740		Plateau
8	QOMS_CAS	86.948	28.365	4276		Plateau
9	SACOL	104.137	35.946	1965		Plateau
10	Lhasa	91.0876	29.6476	3678		Plateau
11	Nanjing	118.9572	32.1147	52		Low altitude plain
12	Changchun	125.396	44	207	Cropland	Low altitude plain
13	XiangHe	116.962	39.754	36		Low altitude plain
14	Xingtai	114.36	37.182	185		Low altitude plain
15	Hefei	117.1622	31.9047	36		Low altitude plain
16	Kashi	75.9304	39.5043	1320		Tableland
17	Minqin	103.0887	38.6328	1589		Plateau
18	Zhangye	100.3643	38.8544	1364		Plateau
19	Beijing	116.381	39.977	92	Urban	Low altitude plain
20	Beijing_PKU	116.31	39.992	53		Low altitude plain
21	Beijing_RADI	116.379	40.005	59		Low altitude plain
22	Beijing-CAMS	116.317	39.933	106		Low altitude plain
23	Hong_Kong_PolyU	114.18	22.303	30		Mountian
24	Shijiazhuang-CHEY	114.55	38	88		Low altitude plain
25	Shijiazhuang-SZF	114.458	38.017	158		Low altitude plain
26	XuZhou-CUMT	117.142	34.217	59		Low altitude plain
27	Chengdu	103.9891	30.5839	510		Low altitude plain
28	Guangzhou	113.3811	23.069	28		Low altitude plain
29	Haikou	110.3267	19.9903	22		Low altitude plain
30	Harbin	126.6141	45.7051	223		Tableland
31	Shanghai	121.4811	31.2841	84		Low altitude plain
32	Xian	109.0006	34.2228	389		Tableland
33	Dunhuang	94.794	40.038	1300	Bare land	Low altitude plain
34	Taihu	120.215	31.421	20	Water	Low altitude plain
35	Sanya	109.3786	18.29	29		Low altitude plain
36	Zhoushan	122.1897	29.9944	29		Low altitude plain

3. Methodology

3.1. Evaluation approach

Since AERONET and SONET do not provide the corresponding spectral AOD measurements at 550 nm, instead of using the Ångström algorithm approach, the more robust second-order polynomial fit approach (Eq. (1)) is selected to interpolate the 550-nm AOD measurements based on the AOD measurements at 870 nm, 675 nm, 500 nm, and 440 nm (Sayer et al., 2019; Wei et al., 2020). For spatiotemporal matching, the AOD real value is defined as the average of at least two AOD measurements within ±30 min of the satellite overpass time (13:30 local time), and the AOD retrieval value refers to the average of all effective satellite-retrieved AOD values within the sampling window (3 × 3 pixels) centered on each monitoring station (Sayer et al., 2019). Traditional statistics metrics mainly include the correlation coefficient (R), the bias, the mean absolute error (MAE, Eq. (2)), the root mean square error (RMSE, Eq. (3)), the relative mean bias (RMB, Eq. (4)), and the widely used AOD expected errors (EE, Eq. (5), Levy et al., 2013).

$$\log(AOD_{550}) = a_0\log(550) + a_1\log(550)^2 + b \tag{1}$$

$$\mathrm{MAE} = \frac{1}{n}\sum_{i=1}^{n}\left|AOD_{(Satellite)i} - AOD_{(Ground)i}\right| \tag{2}$$

$$\mathrm{RMSE} = \sqrt{\frac{1}{n}\sum_{i=1}^{n}\left(AOD_{(Satellite)i} - AOD_{(Ground)i}\right)^2} \tag{3}$$

$$\mathrm{RMB} = \frac{1}{n}\sum_{i=1}^{n}\left(AOD_{(Satellite)i} \Big/ AOD_{(Ground)i}\right) \tag{4}$$

$$\mathrm{EE} = \pm\left(0.05 + 0.2 \times AOD_{Ground}\right) \tag{5}$$

where a_0, a_1, and b are regression coefficients, n is the sample number of AOD matches, $AOD_{(Satellite)i}$ indicates AOD retrievals of VIIRS (EDR and DB) and Aqua MODIS (DT and DB) products, $AOD_{(Ground)i}$ refers to AOD measurements from AERONET and SONET.

3.2. Spatiotemporal analysis

For spatial analysis, monthly AOD maps are averaged from daily VIIRS EDR and DB AOD retrievals at each grid (at least 20% of AOD values are available per month). For temporal analysis, the deseasonalized monthly AOD anomalies are used to calculate the aerosol trends based on the linear regression approach, and the regressed slope refers to the monthly AOD trend (Wei et al., 2019c). Furthermore, the statistical significance of the AOD trend is tested using the MK (Manner-Kendall) nonparametric method (Eqs. (6)–(9)).

$$S = \sum_{i=1}^{n-1}\sum_{j=n+1}^{n} sgn\left(X_j - X_i\right) \tag{6}$$

$$sgn\left(X_j - X_i\right) = \begin{cases} +1, & if\ \left(X_j - X_i\right) > 0 \\ 0, & if\ \left(X_j - X_i\right) = 0 \\ -1, & if\ \left(X_j - X_i\right) < 0 \end{cases} \tag{7}$$

$$Var(S) = \frac{n(n-1)(2n+5) - \sum_{p=1}^{q} t_p\left(t_p - 1\right)\left(2t_p + 5\right)}{18} \tag{8}$$

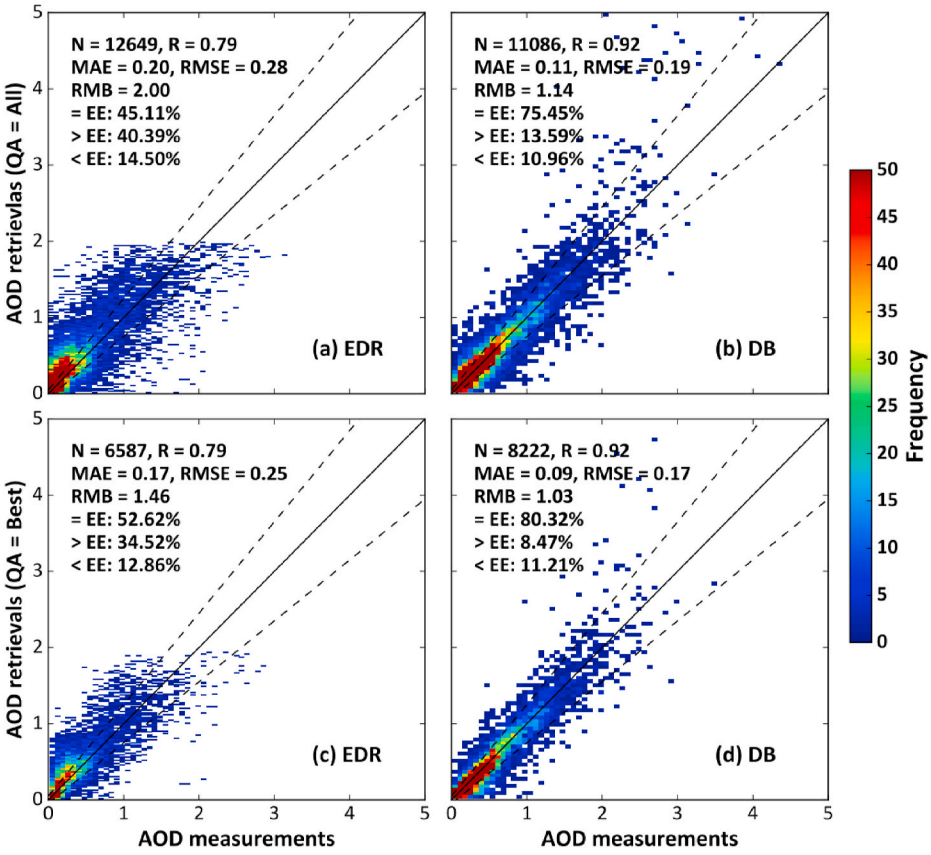

Fig. 2. Evaluation of VIIRS EDR (a, c) and DB (b, d) AOD retrievals with all (QA = All, top) and the best (QA = Best, bottom) quality against ground measurements from 2013 to 2018 in China. The dash line refers to the expected error envelope (EE = ±(0.05 + 0.2 × AOD_{Ground})); the solid line refers to the 1:1 line. N = the number of AOD matchups, R = the correlation coefficient, MAE = the mean absolute error, RMSE = the root mean square error, RMB = the relative mean bias.

$$Z = \begin{cases} \dfrac{S-1}{\sqrt{Var(S)}}, & if\ S > 0 \\ 0, \quad if\ S = 0 \\ \dfrac{S+1}{\sqrt{Var(S)}}, & if\ S < 0 \end{cases} \tag{9}$$

Where S is the statistical value, Var (S) is the variance, X_j and X_i are the deseasonalized monthly AOD anomalies in the jth and ith month, respectively. Only when the standardized test statistics $|Z| > |Z_{(1-\alpha/2)}|$, the AOD trend is significant at the level of 99%, 95%, and 90% when the $|Z_{(1-\alpha/2)}|$ equal to 2.58, 1.96 and 1.65, respectively.

4. Validation and comparison against ground-based measurements

4.1. Spatial-scale validation

4.1.1. National performance

Fig. 2 illustrates the overall comparison of VIIRS EDR and DB AOD retrievals at different quality levels with ground measurements in the whole of China. After quality control, although the number of the data samples generally decreases, both EDR and DB retrievals show significant improvement, where the RMSEs and MAEs have been decreased by 10–11% and 15–19%, respectively. The fraction of EDR and DB AOD matches falling within EE is increased by 17% and 7%. In addition, the overestimations in AOD estimates have been decreased for these two products, especially for the EDR product (RMB = 2.00). Generally, DB AOD retrievals (QA = Best) shows much better performance with an increasing number of matchups, correlation, and fraction within EE by 25%, 17%, and 53% compared to EDR AOD (QA = Best) retrievals; RMSE, MAE, and RMB have also been decreased by 32%, 47%, and 42%, respectively. Notably, VIIRS EDR AOD retrievals have a narrower range from 0 to 2, and yield overall underestimations under high aerosol loadings. By contrast, DB AOD retrievals are extended with a wider range from 0 to 5, and the data samples are closer to the 1:1 line, allowing capturing severely polluted events in China. The reason may be that the DB algorithm has significant refinements in surface reflectance estimation, aerosol model assumption, and cloud screening (Liu et al., 2014; Sayer et al., 2019).

4.1.2. Regional performance

Due to the heterogeneity of surface conditions and aerosol properties, the regional validation and comparison of VIIRS EDR and DB AOD products are also performed (Table 5). The regional division is inherently subjective, but it is generally based on distinct aerosol and surface properties (see Fig. 1). At a regional scale, after quality control, the number of data samples of both EDR and DB AOD products has significantly decreased, and the reduction magnitude of EDR is much greater than DB, especially in the BTH and NW regions. On the other hand, after quality control, the retrieval accuracy of both EDR and DB has overall improved in most regions of China, characterized by the decrease of MAE and RMSE values and the increase of the fractions within EE. Notably, although the EDR accuracy has slightly improved in the BTH and NW regions, the number of data samples has significantly decreased by 45%–65% after quality control. Besides, the DB performance has not improved in the Tibet region after quality insurance. These results illustrate that quality control may not always be helpful at the regional scale (Wei et al., 2018).

In general, VIIRS DB AOD retrievals (QA = Best) show better performance than EDR (QA = Best) in most regions of China. However, both EDR and DB products perform poorly in the Tibet region (R < 0.2), and only 34% and 53% of the data samples fall within EE, showing severe overestimations (RMB > 1.7). On the one hand, Lhasa site (3678 m), NAM_CO site (4740 m), and QOMS_CAS site (4276 m) of the Tibet region belong to complex and heterogeneous surface types, characterized by the crisscross of alpine vegetation, meadow, and desert (Che et al., 2015; Li et al., 2018). Especially for high-altitude areas, this undoubtedly increases the difficulty of both DB and EDR products in surface reflectance estimation. On the other hand, the three aerosol sites are all located in the north of the Himalayas. Affected by the downdraft, they are dry and windy in winter and spring, and thus dust aerosols are transported to these sites. Wind erosion leads to an increase in coarse-mode AOD at these sites, which makes it more difficult for EDR to retrieve dust aerosols (Xu et al., 2014). However, the number of data samples of DB product is approximately 62% and 85% more than the EDR product in the BTH and NW regions. By contrast, in the PRD and Tibet regions, the number of data samples of DB product is less than EDR product by ~65% and ~60%, possibly due to the unreliable cloud screening of the EDR algorithm (Liu et al., 2014). Furthermore, the DB algorithm has higher retrieval accuracy than the EDR algorithm in most areas of China, especially in the BTH region. More importantly, EDR AOD retrievals are significantly overestimated in all regions, especially in the Tebit region (RMB = 3.83). By contrast, except for BTH and Tibet regions, DB AOD retrievals are overall underestimated by 8–11% in the remaining regions of China.

4.1.3. Site-scale performance

Since the ground sites are not evenly distributed, the site-scale performance of VIIRS AOD products is further analyzed (Fig. 3). To be statistically significant, only those sites with more than ten AOD matches are plotted. Before and after quality control, the spatial pattern of VIIRS AOD product retrieval accuracy is similar, but there are still differences in numerical values for individual sites. In general, the retrieval accuracy of both VIIRS EDR and DB AOD products has improved at most sites of China after quality control, i.e., 68–83% and 67–79% of sites show an increase in the correlation and the fraction within EE, and RMSEs and MAEs have decreased at 67–89% and

Table 5
Accuracy statistics of VIIRS EDR and DB AOD retrievals against ground measurements from 2013 to 2018 in each region of China.

Region	QA	VIIRS EDR AOD						VIIRS DB AOD					
		N	R	MAE	RMSE	RMB	= EE	N	R	MAE	RMSE	RMB	= EE
BTH	All	5304	0.82	0.20	0.29	1.14	42.70	5419	0.94	0.10	0.19	1.03	78.46
	Best	2891	0.82	0.19	0.27	1.18	44.41	4682	**0.95**	**0.08**	**0.15**	**1.01**	**81.27**
YRD	All	2415	0.72	0.21	0.32	1.15	42.07	2123	0.82	0.13	0.24	0.94	61.38
	Best	1706	0.69	0.16	0.27	1.07	49.12	1519	**0.79**	**0.13**	**0.24**	**0.92**	**61.49**
PRD	All	716	0.73	0.21	0.30	1.33	44.83	494	0.80	0.13	0.20	0.82	58.91
	Best	520	0.76	0.13	0.20	1.11	56.92	180	**0.88**	**0.09**	**0.13**	**0.91**	**77.22**
NW	All	2135	0.62	0.15	0.22	0.99	37.99	2059	0.90	0.09	0.14	1.02	65.08
	Best	749	0.71	0.14	0.19	1.01	38.85	1385	**0.93**	**0.09**	**0.13**	**0.89**	**67.29**
Tibet	All	1132	0.18	0.20	0.27	4.52	24.12	317	0.28	0.06	0.11	1.40	75.39
	Best	112	0.07	0.14	0.18	3.83	33.93	45	0.14	0.08	0.11	1.78	53.33

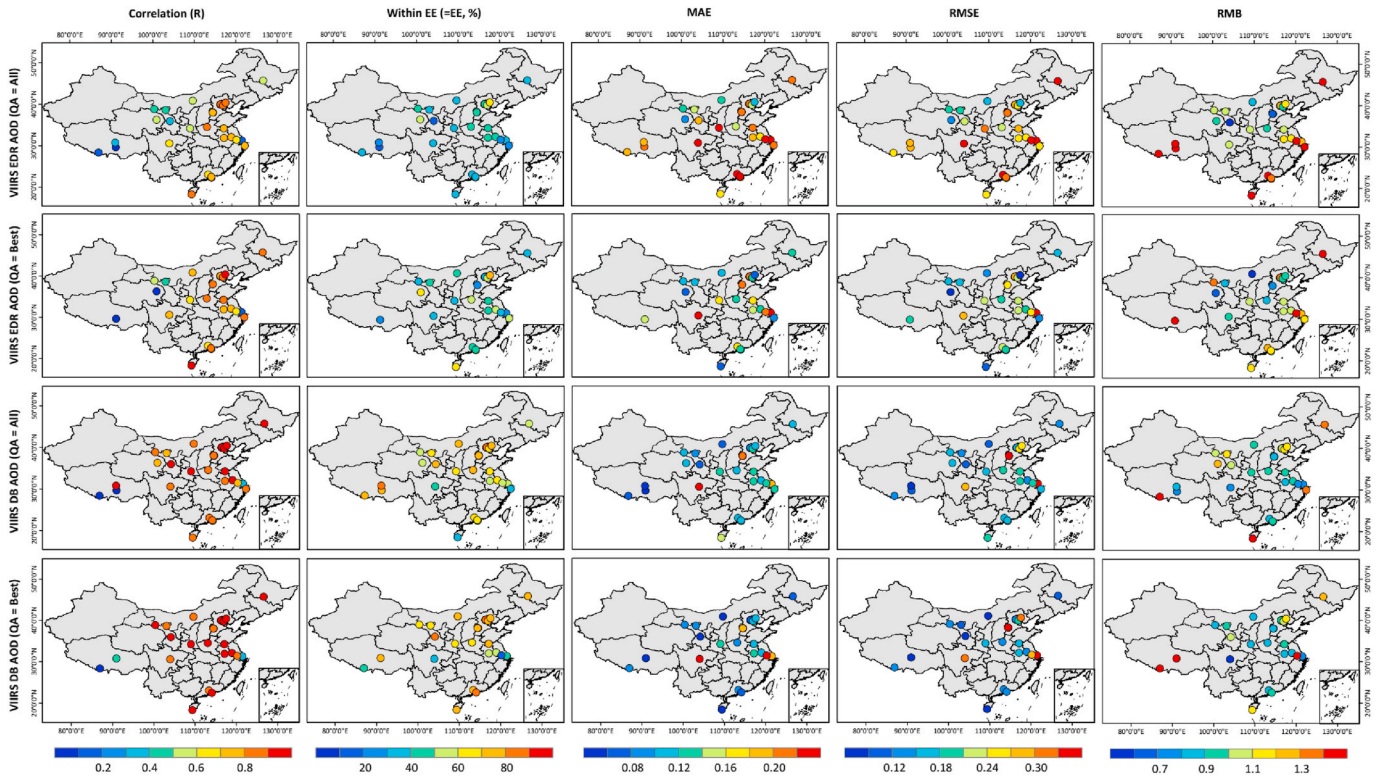

Fig. 3. Comparison of VIIRS EDR (QA = All and Best, row 1–2) and DB (QA = All and Best, row 3–4) AOD retrivals against ground measurements at each site in China. The statistics including correlation, within EE, MAE, RMSE, and RMB are respectively presented in columns 1–5.

67–71% sites, respectively. Nevertheless, the quality control of VIIRS AOD products is not always effective at the site scale. For example, the retrieval accuracy of VIIRS EDR and DB products has not improved at sites of Tibet and some urban sites (i.e., Chengdu and Shanghai). As shown in section 4.1.2, the poor performance of both EDR and DB products in Tibet before and after quality control is caused by the difficulty in surface reflection estimation on heterogeneous surface types with high altitudes and the difficulty in retrieving dust AODs (Xu et al., 2014). In addition, the Chengdu site is located in the Sichuan Basin, where cloudy weather conditions and diverse urban aerosol types make

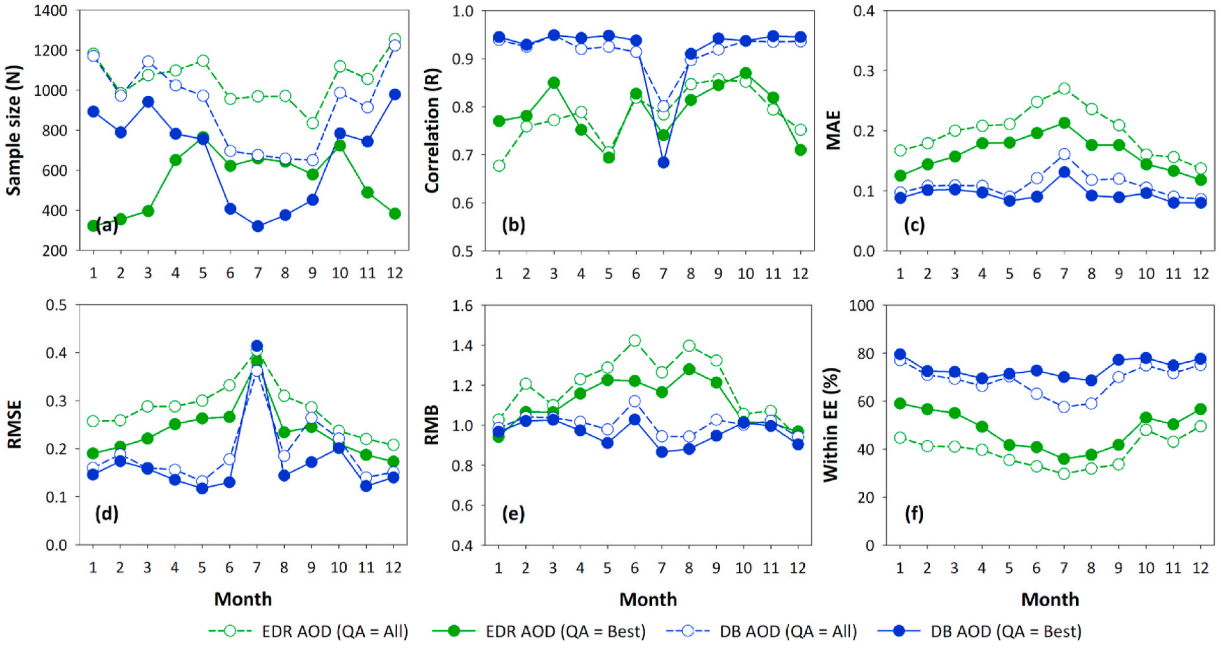

Fig. 4. Comparison of VIIRS EDR (QA = All and Best) and DB (QA = All and Best) AOD products against ground measurements at each month in China from 2013 to 2018. The statistics include (a) sample size, (b) correction, (c) MAE, (d) RMSE, (e) RMB and (f) within EE.

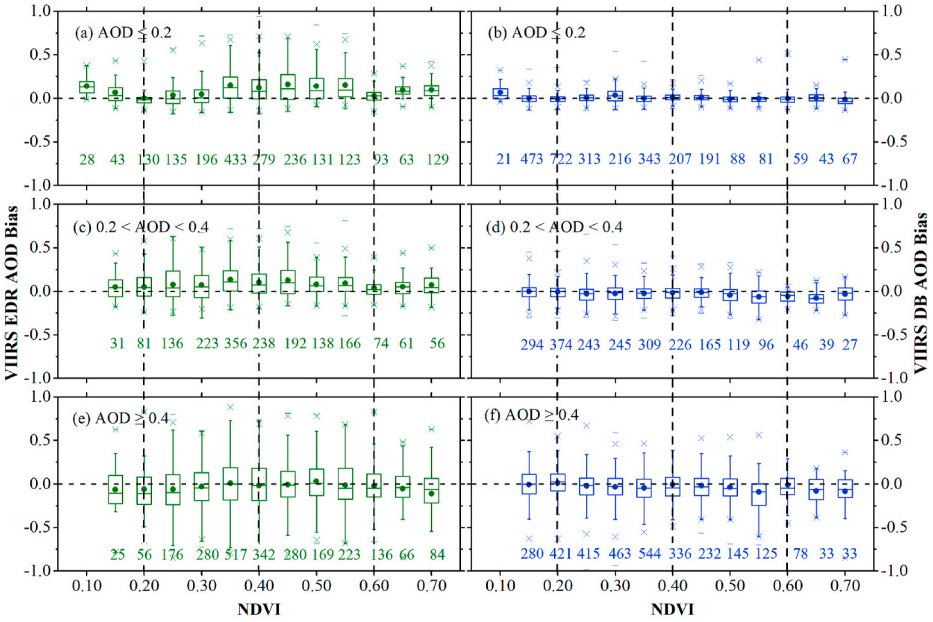

Fig. 5. Boxplot of AOD bias for VIIRS EDR (left) and DB (right) AOD retrievals against ground measurements as a function of NDVI under different aerosol loading conditions in China. The low (AOD $\leq$ 0.2, a-b), moderate (0.2 < AOD < 0.4, c-d) and high (AOD $\geq$ 0.4, e-f) aerosol loading conditions are considered. The number of EDR and DB AOD samples for each bin is listed in green and blue, respectively. (For interpretation of the references to color in this figure legend, the reader is referred to the Web version of this article.)

it difficult for both EDR and DB products to efficiently retrieve AODs here. Similar to Chengdu, the Shanghai station also mainly observes urban aerosols, including black carbon, brown carbon, fine-model components and maritime aerosols (Li et al., 2018), which undoubtedly increases the difficulty of EDR and DB products in aerosol type assessment.

In general, VIIRS EDR AOD retrievals are overall poorly correlated to ground measurements, with only 26–37% of the total sites showing high correlations (R > 0.8). By contrast, VIIRS DB AOD retrievals yield much higher consistency with ground observations, where high correlations (R > 0.8) are observed at approximately 73–90% of the sites in China. However, these sites with low correlations (R < 0.4) are mainly observed in western China. In addition, DB AOD products showing good matching, with more than 68% of the AOD retrievals falling within EE at 63–73% of the sites. However, the EDR AOD retrievals are well-matched with the observations at only 3–20% of the sites in China.

Furthermore, there are similar spatial patterns for estimation uncertainties (i.e., MAE, RMSE) of VIIRS AOD products at the site scale in China. In general, DB shows small MAE and RMSE values less than 0.1 and 0.15 at 57–67% and 60–70% sites, where most of them are located in western and southern China. However, only 3–14% and 3–21% of sites show low MAE and RMSE values for EDR AOD products, respectively. In particular, both EDR and DB AOD products show large estimation uncertainties (e.g., MAE > 0.18, RMSE > 0.28) in main urban sites, including Shanghai, Chengdu, Shijiazhuang-CHEY, and Shijiazhuang-SZF sites, mainly due to numerous anthropogenic aerosols and unfavorable meteorological conditions. Besides, there are 47–50% and 23–27% of the sites have small-biased AOD estimates with small RMB values ranging from 0.9 to 1.1 for DB and EDR AOD retrievals, respectively. Nevertheless, EDR AOD retrievals are severely overestimated (RMB > 1.1) at 57–67% of sites, especially for these sites in the southeast of China and the Tibet region. By contrast, DB AOD retrievals are severely underestimated at approximately 27–33% of the sites, where are mostly located in central China.

4.2. Temporal-scale validation

Fig. 4 plots the monthly variations in the overall accuracy and uncertainty between VIIRS EDR and DB products before and after quality control. Overall, after quality control, although the sample size has decreased, the retrieval accuracy and uncertainty of EDR and DB AOD products have been significantly improved throughout the year but present obvious seasonal variations. In general, EDR and DB products show a smaller number of AOD matchups in the middle of the year, mainly due to the high cloud coverage in the rainy season (Mhawish et al., 2019). In terms of correlation, DB retrievals are highly correlated (R > 0.9) to ground measurements in the whole year, except for July. However, EDR retrievals present a more significant seasonal change with lower R values than DB over time. In terms of uncertainty, MAE and RMSE present similar unimodal curves with the peaks in July, which is mainly due to the high aerosol loadings caused by straw burning and aerosol hygroscopic growth in summer (Xia et al., 2016). In terms of RMB, EDR products always show significant overestimations in most months throughout the year, and the peaks are observed around the summer. However, DB retrievals show lower and more stable RMB values below 1.1 for the whole year. Moreover, EDR and DB products show similar seasonal variations in terms of the fraction within EE, and the lower fractions are observed in these months in the middle of the year.

5. Error and uncertainty analysis of VIIRS AOD products

To further reveal the uncertainty sources of VIIRS AOD products, the section focuses on the sensitivity of EDR and DB algorithms to different land surface conditions and aerosol optical-microphysical properties. Only EDR and DB products passing the quality assurance (QA = Best) are used hereafter.

5.1. Related to varying surface conditions

5.1.1. NDVI

Minor errors in surface reflectance estimations may cause large deviations in AOD retrievals, especially under low aerosol loading conditions. Therefore, the sensitivity of EDR and DB products to NDVI changes is investigated under low (AOD $\leq$ 0.2), moderate (0.2 < AOD < 0.4), and high (AOD $\geq$ 0.4) aerosol loading scenarios. Here, NDVI is used as a proxy of surface conditions, which are classified into four types: permanently arid areas (NDVI $\leq$ 0.2), arid and semi-arid areas with seasonal variations of vegetation (0.2 < NDVI < 0.4), moderate vegetation covers (0.4 < NDVI < 0.6) and dense vegetation covers (NDVI $\geq$ 0.6). In order to be consistent with AOD validation, the spatial window of NDVI has also selected as 18 km × 18 km, and the daily NDVI is

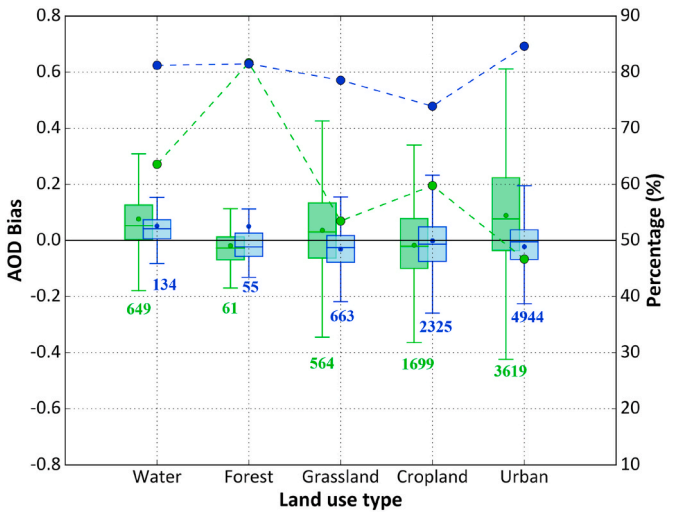

Fig. 6. AOD bias (boxplots) and the fraction of AOD matches falling within the EE envelopes (curves) for VIIRS EDR (green) and DB (blue) AOD retrievals against ground measurements at different land use types in China. The number of EDR and DB AOD samples for each bin is listed in green and blue, respectively. (For interpretation of the references to color in this figure legend, the reader is referred to the Web version of this article.)

interpolated from the MODIS NDVI product using the spline interpolation. To be significant, the number of EDR and DB AOD retrievals in each bin must be greater than 20.

Fig. 5 illustrates EDR and DB AOD biases as a function of NDVI under different aerosol loading scenarios. In general, DB AOD bias presents little sensitivity to NDVI under all aerosol loadings, while the variations of EDR AOD bias become more complicated. For the low aerosol loading scenario (Fig. 5 a-b):, when NDVI $\leq$ 0.2, EDR AOD bias is continuously positive and the standard deviation gradually narrows down with the NDVI increase, while the DB AOD bias is more stable ($<$ 0.07); when 0.2 $<$ NDVI $<$ 0.4, EDR retrievals show large positive biases, but the DB bias is always stable around 0.01; when 0.4 $<$ NDVI $<$ 0.6, although the EDR bias is still large, the spread of bias is fairly stable around 0.15; when NDVI $\geq$ 0.6, EDR and DB biases become closer to zero and the standard deviations narrow down. For the moderate aerosol loadings (Fig. 5c–d), EDR and DB products show similar AOD bias patterns and variations but with larger numerical values than those results of the low-aerosol-loading conditions. However, for the high aerosol loadings (Fig. 5 e-f), although the standard deviations become larger, the biases of both EDR and DB AOD products are closer to zero, indicating that the sensitivity of EDR and DB AOD biases to NDVI is not significant.

5.1.2. *Land use type*

Here, the surface is divided into five main types, including water, forest, grassland cropland, and urban according to the MODIS land use cover product. Fig. 6 shows the performance of EDR and DB AOD retrievals at different land-use types. EDR product shows the highest accuracy in the forest with the smallest bias, and up to 80% of AOD matches falling within EE, followed by the water, cropland, and grassland. The reason is that the VIIRS EDR product is designed based on the MODIS DT algorithmic heritage, which is suitable for aerosol retrieval over dark surfaces (Liu et al., 2014; Huang et al., 2016). In contrast, the

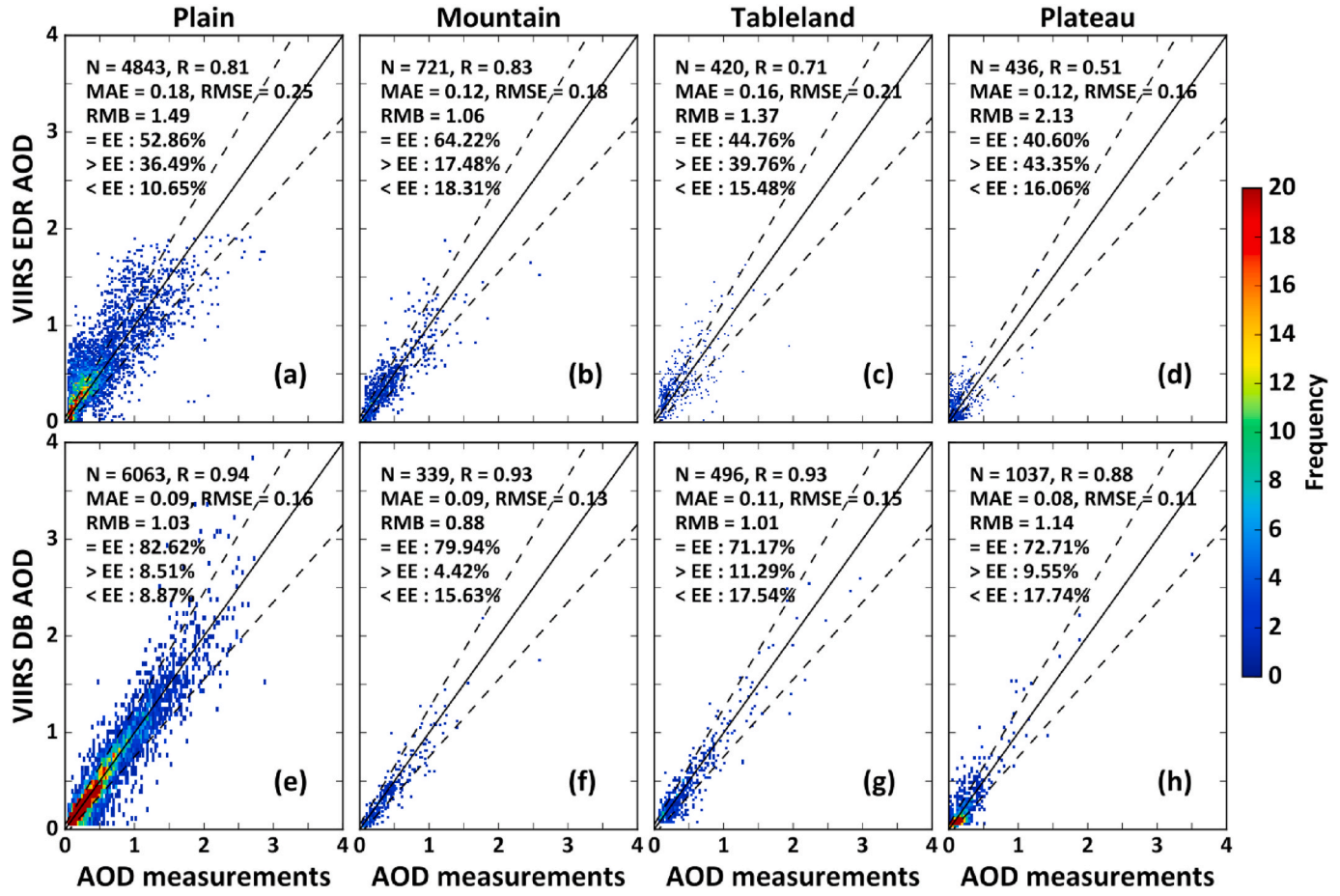

Fig. 7. Evaluation of VIIRS EDR (top) and DB (bottom) AOD retrievals against ground measurements over (a, e) plain, (b, f) mountain, (c, g) tableland, and (d, h) plateau landform types.

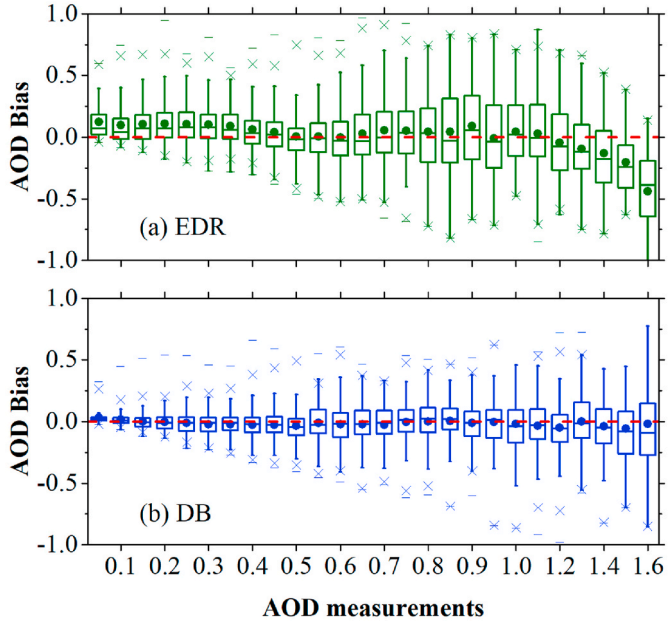

Fig. 8. Boxplot of AOD bias for VIIRS (a) EDR and (b) DB AOD retrievals against ground measurements at different pollution levels in China.

EDR product shows the worst accuracy over the bright urban surface with a large positive bias, and only 47% of the data samples fall within EE. However, the VIIRS DB algorithm is developed to retrieve aerosols over all snow-free land surfaces (Hsu et al., 2019); thus, the DB product shows satisfactory retrieval accuracy for all land-use types. In general, DB retrievals are overall more accurate than DT retrievals with smaller biases and higher fractions of the data samples falling within the EE at most land-use types in China, especially for urban, where the fraction of DB AOD retrievals within EE is as high as 84%, and the bias is close to zero.

5.1.3. Landform type

Fig. 7 plots the evaluation of EDR and DB AOD products over the four landform types, including plain, mountain, tableland, and plateau. In general, DB shows good performance in all landform types in terms of all statistics, while the pattern of EDR becomes more complicated. EDR presents the best performance in mountainous landforms, with a high correlation (R = 0.83) and up to 64% of AOD matches falling within EE. The reason may be that vegetation surfaces such as forests dominate the mountainous areas (Sayer et al., 2019). On the contrary, EDR shows the worst performance in plateau landforms, where only about 41% of AOD matches fall within EE, and more than 43% of EDR retrievals are overestimated. The main reason is that these ground stations are mainly distributed in the Loess Plateau and the Tibet Plateau, where bare bright surfaces and dust aerosols dominate (Huang et al., 2007). Therefore, EDR performs poorly in plateau landforms. However, the DB algorithm shows satisfactory performance in all landform types, especially in the plain landform, where up to 83% of DB AOD matches fall within EE. The reason may be that the stations of the plain landform are mainly located around urban agglomerations with bright surfaces.

5.2. Related to varying atmospheric conditions

5.2.1. Air pollution level

Fig. 8 shows the EDR and DB AOD retrieval biases at different pollution levels in China. AOD ground measurements are divided into bins with a width of 0.1. In general, DB shows a very small mean AOD bias close to zero under all aerosol loadings, while the bias pattern of EDR is more complicated. Especially for AOD < 0.4, the mean EDR AOD bias is always positive, indicating that EDR AODs are significantly overestimated at low air pollution levels. For 0.4 < AOD < 1.0, although the mean EDR AOD bias is positive, it is closer to zero. However, for AOD > 1.0, the mean EDR AOD bias becomes more negative with the growth of aerosol loading, suggesting that EDR AODs are underestimated at high air pollution levels. The reason may be that the inappropriate assumption of aerosol properties leads to a large bias on EDR retrievals, especially at high-polluted levels (Huang et al., 2016; Hsu et al., 2019).

5.2.2. Aerosol particle size

Improper assumptions of aerosol optical and microphysical properties usually lead to considerable uncertainty in the satellite retrieval of the top-of-atmosphere reflectance, especially under high aerosol

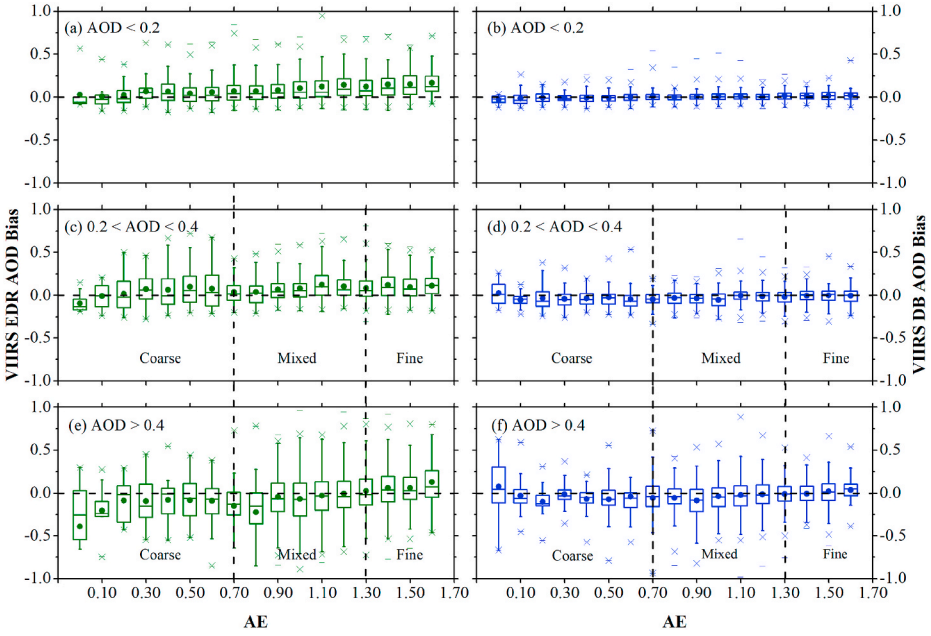

Fig. 9. Boxplot of AOD bias for VIIRS EDR (left) and DB (right) AOD retrievals against ground measurements as a function of Ångström exponent (AE) measurements undert different aerosol loadings in China. The low (AOD ≤ 0.2, a-b), moderate (0.2 < AOD < 0.4, c-d) and high (AOD ≥ 0.4, e-f) aerosol loading conditions are considered. The vertical black dash lines separate the coarse (AE > 0.7), mixed (0.7 < AE < 1.3) and fine (AE > 1.3) aerosol fractions.

loadings (Hsu et al., 2019; Sayer et al., 2014). Aerosol AE index characterizes aerosol particle size, and a larger AE means a smaller aerosol particle size. Here, we divide aerosols into four types according to AE (Sayer et al., 2014), including the coarse-mode aerosols dominated by mineral coarse (AE > 0.7), mixed-mode aerosols (0.7 < AE < 1.3), and fine-mode aerosols likely dominated by smoke or industrial pollution (AE > 1.3).

Under low aerosol loadings (AOD ≤ 0.2), the EDR AOD biases are always positive and continuously increases with AE values, indicating that it is more sensitive to aerosol particle size than DB (Fig. 9a). By contrast, DB presents a fairly stable mean bias (~0.005), suggesting that it is less sensitive to aerosol particle size compared to NDVI (Fig. 9b). Additionally, the performance of EDR is far worse than DB, as only 46% of EDR AOD matches fall within EE, and a large number of the EDR AOD retrievals are overestimated (Table 6).

Under moderate (0.2 < AOD < 0.4, Fig. 9c) and high aerosol loading conditions (AOD ≥ 0.4, Fig. 9e), EDR is more sensitive to the aerosol particle size and shows much worse accuracy in retrieving coarse-mode aerosols, showing a smaller number of data samples, larger MAE and RMSE values, and only 38%–40% of AOD matches falling within EE. It is worth noting that the coarse-mode EDR AOD retrievals are overestimated by 19% under moderate aerosol loadings, while they are underestimated by 15% under high aerosol loadings. By contrast, DB AOD retrievals are less influenced by the aerosol particle size under moderate (Fig. 9d) and high aerosol loadings (Fig. 9f), showing small MAE and RMSE values and high fractions of 66%–83%.

Table 6
Accuracy statistics of VIIRS EDR (QA = Best) and DB (QA = Best) AOD retrievals against ground measurements over different aerosol types.

Metrics	AOD	< 0.2	0.2–0.4			> 0.4		
	$AE_{440\text{-}870}$	/	Coarse	Mixed	Fine	Coarse	Mixed	Fine
N	EDR	2219	242	822	829	145	1385	944
	DB	2874	383	1012	810	284	1786	1072
MAE	EDR	0.134	0.167	0.131	0.135	0.257	0.223	0.200
	DB	0.042	0.087	0.072	0.071	0.160	0.163	0.119
RMSE	EDR	0.16	0.20	0.15	0.14	0.27	0.27	0.26
	DB	0.05	0.10	0.09	0.10	0.24	0.24	0.17
Bias	EDR	0.104	0.057	0.089	0.103	−0.143	−0.049	0.053
	DB	0.005	−0.033	−0.023	−0.007	−0.029	−0.033	0.000
RMB	EDR	2.073	1.189	1.337	1.383	0.856	0.966	1.097
	DB	1.170	0.880	0.915	0.980	0.946	0.955	0.994
= EE (%)	EDR	46.15	40.08	56.69	54.52	38.36	57.40	61.02
	DB	85.28	66.06	76.48	77.53	77.71	77.11	83.12

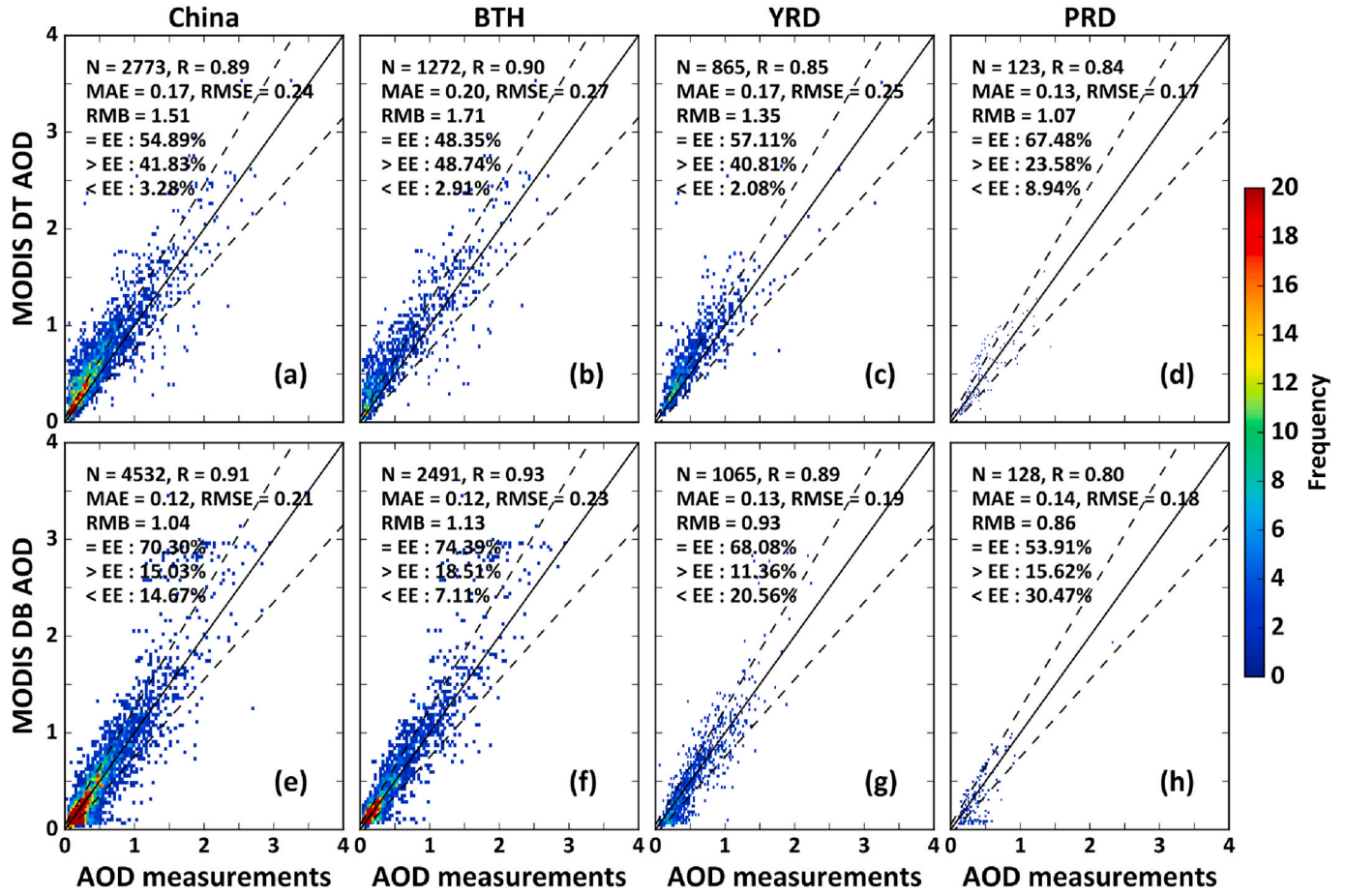

Fig. 10. Validation of MODIS DT (top) and DB (bottom) AOD retrievals against ground measurements over China (a, e), BTH (b, f), YRD (c, g), and PRD (d, h).

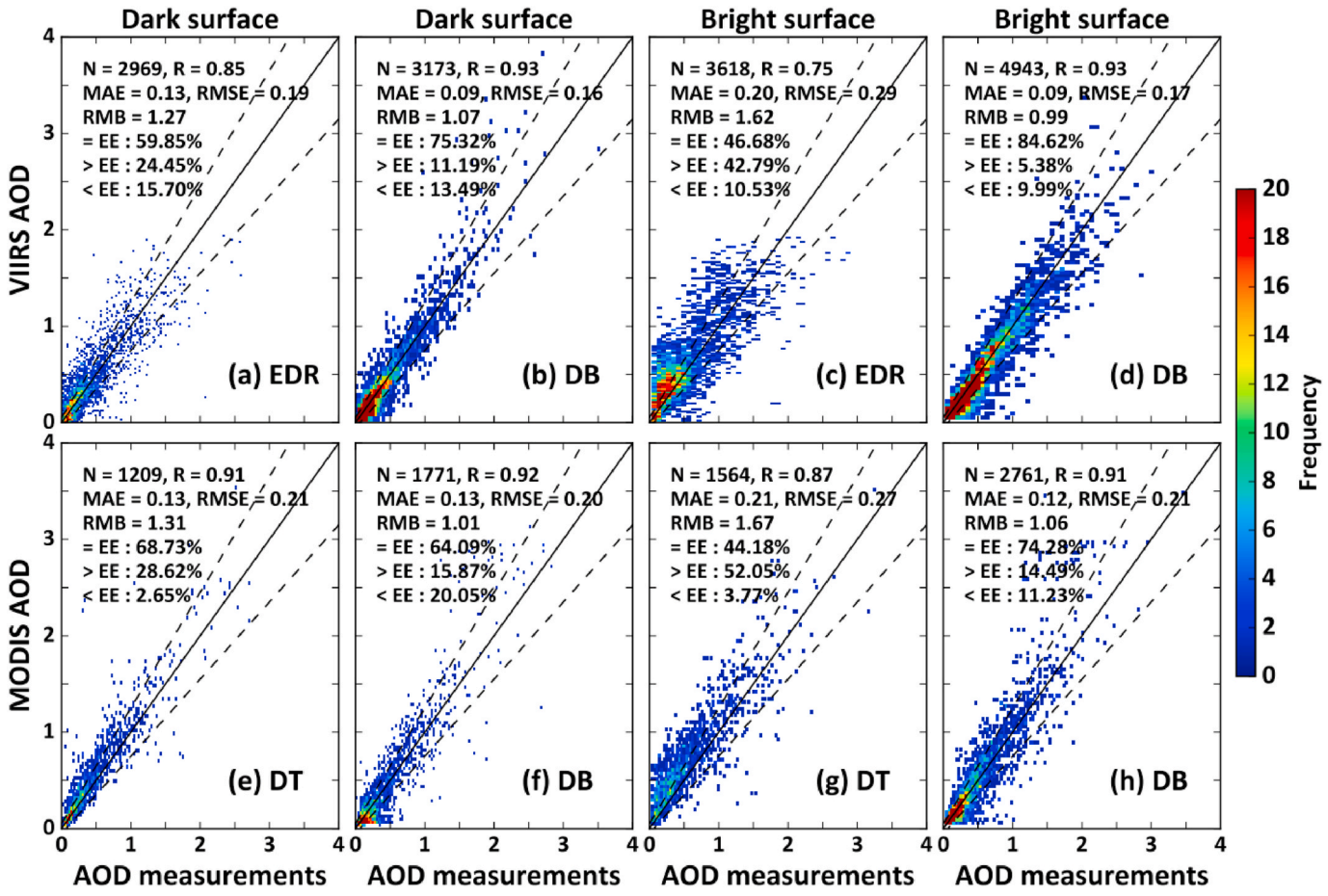

Fig. 11. Evaluation of VIIRS (top) and MODIS (bottom) AOD retrievals against ground measurements over dark (a, b, e and f) and bright (c, d, g and h) surfaces from 2013 to 2018.

6. Comparison between VIIRS and MODIS AOD products

Given the sensor characteristics and common algorithmic heritage between VIIRS and MODIS, VIIRS is expected to continue to provide global multispectral aerosol retrievals for decades after MODIS (Liu et al., 2014). Here, we compare VIIIRS EDR and DB products with

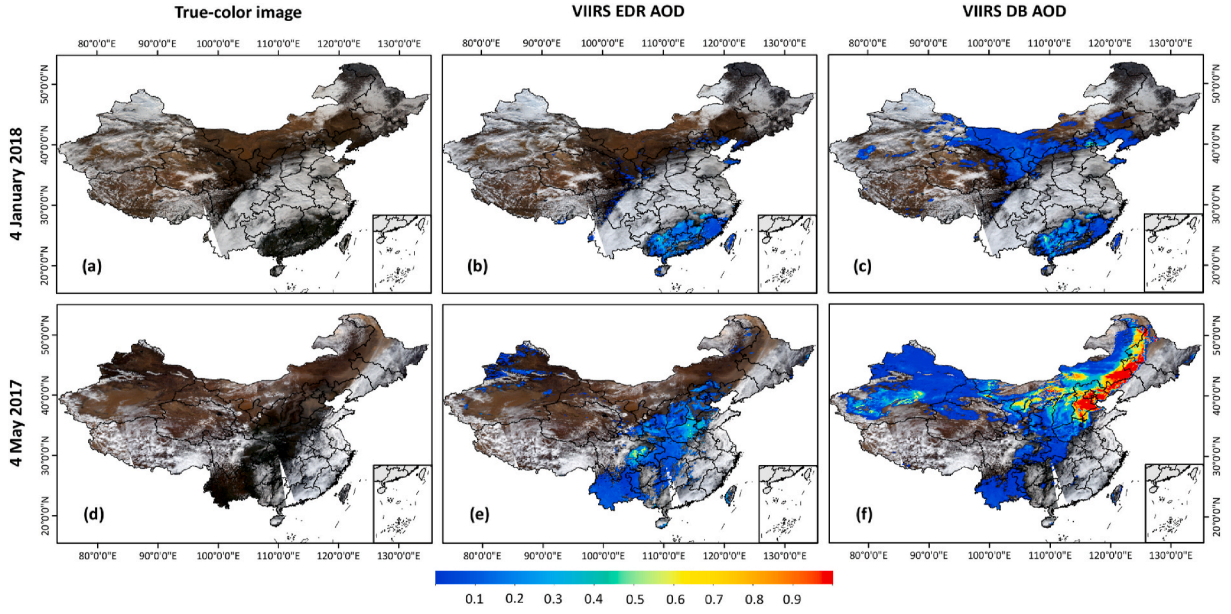

Fig. 12. (a) True-color image, (b) VIIRS EDR and (c) DB AOD data sets under a light pollution event on January 4, 2018. (d–f) show those under a heavy dust pollution event on May 4, 2017. (For interpretation of the references to color in this figure legend, the reader is referred to the Web version of this article.)

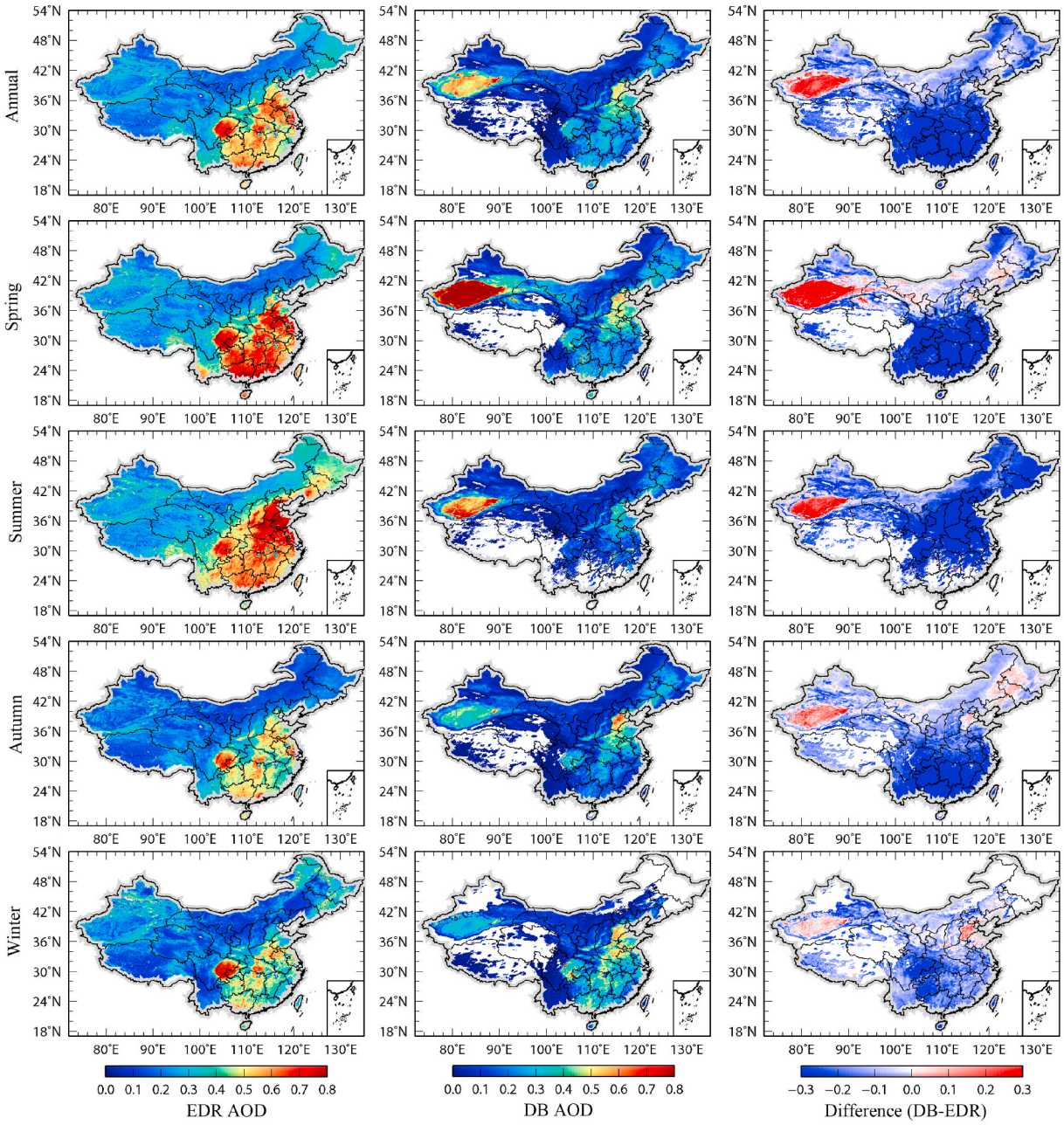

Fig. 13. Spatial distributions of annual and seasonal mean VIIRS EDR (left), DB (middle), and their difference (right) AODs during 2013–2018 in China, respectively.

MODIS Aqua C6.1 DT and DB products in different regions of China (Fig. 10). Generally, MODIS DB AOD retrievals are more accurate than MODIS DT AOD with a higher correlation, a lower MAE and RMSE, and a higher fraction within EE in China. Moreover, MODIS DT tends to be severely overestimated by 51%. MODIS DT and DB algorithms present similar performances with VIIRS EDR and DB products (Fig. 2) in China. The reason is closely attributed to the common algorithmic heritage between VIIRS and MODIS. At the regional level, MODIS DB performs better than MODIS DT with all better statistical metrics in the BTH and YRD regions. By contrast, the MODIS DT product shows higher accuracy than MODIS DB in the PRD region, showing a larger fraction of 67%, and lower estimation uncertainties (e.g., MAE = 0.13, RMSE = 0.17). It should be noted that 14% of MODIS DB AOD retrievals are underestimated. In conclusion, VIIRS EDR (DB) products show comparable performance with MODIS DT (DB) products in China and most regions (Fig. 2 and Table 5), suggesting that VIIRS can extend the long-term aerosol records together with MODIS.

Fig. 11 illustrates the comparison results of VIIRS and MODIS AOD retrievals against AOD ground observations over dark and bright surfaces. VIIRS EDR and MODIS DT products show good accuracy over dark surfaces with small MAE and RMSE values, and approximately 60%–69% of the data samples fall within the EE. However, they perform much poorly over bright surfaces, showing larger estimation uncertainties (i.e., MAE $>$ 0.20, RMSE $>$ 0.27), and the AOD retrievals are significantly overestimated (RMB $>$ 1.62). Additionally, VIIRS and MODIS DB products show similar performance with close evaluation metrics compared to EDR and DT products over dark surfaces. By contrast, they perform much better over bright surfaces with much lower estimation uncertainties (i.e., MAE $<$ 0.12, RMSE $<$ 0.21), and about 1.6–1.9 times more data samples falling within the EE. The finding reveals the superior performance of the VIIRS DB algorithm over both dark and bright surfaces.

7. Spatiotemporal characteristics of VIIRS AOD products

7.1. Spatial coverage and distribution

Fig. 12 illustrates the spatial distributions of VIIRS EDR and DB AOD products under a light pollution event on January 4, 2018, and a heavy dust event on May 4, 2017, in China, respectively. In general, DT and DB products have a relatively consistent spatial pattern in aerosol loadings, but there are obvious differences in spatial coverage. Both EDR and DB products can provide similar spatial distributions of aerosol information under low-polluted conditions. However, they show a large number of missing values in high latitudes of northern China and high altitudes of the Tibetan Plateau because both EDR and DB algorithms cannot work on snow/ice surfaces (Hsu et al., 2019). More importantly, DB enables to retrieve extremely high AOD values under high-polluted dust conditions where were occurred in the North China Plain, Northeast China, and the Taklamakan Desert. By contrast, EDR fails to capture the severe air pollution event, showing numerous missing values (Fig. 12e–f).

Fig. 13 shows the spatial patterns of multi-year annual and seasonal average VIIRS EDR, DB, and their differences (DB-EDR) AODs in China from 2013 to 2018. The corresponding statistical results are further listed in Table 7. In general, both EDR and DB capture relatively high AOD retrievals in the BTH, YRD, and Sichuan Basin regions with dense populations and frequent industrial activities. However, EDR AODs are much higher than DB AODs in these areas because EDR retrievals are severely overestimated by 46% with reference to the ground measurements (Fig. 2). Especially in summer, their AOD difference reaches up to 0.28–0.55, mainly due to the algorithm differences in addressing aerosol hygroscopic growth during the rainy season (Mhawish et al., 2019). On the contrary, in the Taklamakan Desert, DB AOD values are much higher than EDR, with the largest difference (>0.2) in spring. The reason is that unlike EDR, DB has a good ability to retrieve dust aerosols over bright surfaces, especially in deserts (Sayer et al., 2018, 2019). However, DB products show a large number of missing values in Tibet and Northeast China due to permanent snow/ice covers, especially in winter. By contrast, EDR has effective but unreliable AOD values in these regions, which may be due to inaccurate pixel screening (Liu et al., 2014; Huang et al., 2016). In addition, our results illustrate that spatial distributions of VIIRS EDR and DB products are highly consistent with MODIS DT and DB products across China (Liu et al., 2019).

Fig. 14 illustrates the spatial frequency of VIIRS EDR and DB AOD retrievals and their difference in China from 2013 to 2018. The results show that the retrieval frequency of EDR and DB AOD products is higher in the BTH region and Northeast China due to fewer clouds. However, in the NW region, especially in the Taklamakan Desert, the retrieval frequency of the EDR AOD product is relatively low < 90 days/year, while the DB AOD product shows a much higher retrieval frequency > 210 days/year. The main reason is that the EDR algorithm has a poor ability to retrieve aerosols in bright desert areas. Furthermore, there are also some differences in retrieval frequency at the seasonal level, where DB has a lower AOD retrieval frequency in summer, mainly due to a large number of clouds in the rainy season (Liu et al., 2019). However, EDR has a lower AOD retrieval frequency in winter, especially in the Sichuan Basin and the Taklamakan Desert. In general, except for northwest China, the EDR AOD retrieval frequency is overall higher than DB throughout the year in most areas of China.

Table 7
Statistics of annual and seasonal mean AOD loads over China and each region calculated from VIIRS EDR and DB AODs product during 2013–2018.

Region	Data	Annual	Spring	Summer	Autumn	Winter
China	EDR	0.32 ± 0.14	0.35 ± 0.17	0.40 ± 0.16	0.26 ± 0.14	0.27 ± 0.14
	DB	0.14 ± 0.12	0.21 ± 0.19	0.10 ± 0.12	0.12 ± 0.11	0.15 ± 0.13
BTH	EDR	0.37 ± 0.13	0.34 ± 0.15	0.57 ± 0.18	0.33 ± 0.14	0.23 ± 0.10
	DB	0.21 ± 0.15	0.24 ± 0.16	0.17 ± 0.11	0.23 ± 0.17	0.21 ± 0.17
YRD	EDR	0.54 ± 0.11	0.35 ± 0.17	0.40 ± 0.16	0.26 ± 0.14	0.27 ± 0.14
	DB	0.19 ± 0.08	0.21 ± 0.09	0.12 ± 0.08	0.17 ± 0.08	0.24 ± 0.10
PRD	EDR	0.56 ± 0.07	0.70 ± 0.08	0.60 ± 0.09	0.51 ± 0.08	0.42 ± 0.07
	DB	0.18 ± 0.06	0.21 ± 0.07	0.05 ± 0.08	0.13 ± 0.04	0.23 ± 0.08

7.2. Temporal variation and trend

Fig. 15 displays the linear AOD trends derived from EDR and DB products across China from 2013 to 2018. Areas where the AOD trends did not pass the significance test ($p > 0.1$) are marked as blank. The results show that both EDR and DB products show significantly decreasing AOD trends > 0.01 per year in Eastern and Southern China with heavy anthropogenic aerosol loadings. This is closely related to the effective implementation of China's energy-saving and emission reduction policies in recent years (Zhang et al., 2017; Leeuw et al., 2018). However, EDR shows overall increasing AOD trends in Western China, especially in Tibet ($p < 0.01$), while DB presents non-significant AOD trends in these areas. Nevertheless, due to the inadaptability of the EDR algorithm in the bright surfaces, the observed trends may not be reliable.

Fig. 16 investigates the monthly variations of VIIRS EDR and DB AOD anomalies across China and each region from 2013 to 2018. Both EDR and DB presented similar temporal AOD variations with a significant downward trend equal to −0.0008 per year ($p < 0.01$) in the whole of China. However, there are noticeable differences in the three main typical urban agglomerations, where these two products show similar decreasing AOD trends by −0.0204 and −0.0168 per year at the same significant level ($p < 0.01$) in the YRD region, respectively. In addition, similar conclusion can be obtained in the PRD region, where the AOD trends are −0.0228 ($p < 0.01$) and −0.0096 ($p < 0.05$) per year, respectively. However, a large difference exited in the BTH region, where DB AOD is significantly decreased by −0.0156 per year ($p < 0.01$), while no similar aerosol trend was observed for EDR AOD product (Trend = −0.0024, $p = 0.49$).

Therefore, to explore the authenticity of different aerosol products in describing the aerosol change in the BTH region, we collected and calculated the real aerosol trends using the same method at three long-term AERONET monitoring stations, including two typical urban sites (i.e., Beijing and Beijing-CAMS) and one vegetated site (i.e., Xianghe) in this area (Fig. 17). The results show that the EDR products show the same significant decreasing AOD trends as the ground measurements in two urban sites (Fig. 17a–b); on the contrary, their AOD trends are totally opposite in the vegetated site (Fig. 17c). However, the DB products exhibit more similar AOD variations with the observations with closer significant decreasing trends at all three sites. These findings demonstrate that DB products can capture more accurate aerosol changes compared to the EDR products in China.

8. Conclusion

In this study, we perform an initial and comprehensive evaluation of VIIRS DB and EDR products throughout China from 2013 to 2018. The overall accuracy assessment suggests that both EDR and DB products have significantly improved after quality assurance (QA) control. DB (QA = Best) shows satisfactory retrieval accuracy with high correction (R = 0.92), and up to 80.32% of AOD matches falling within EE, while only 52.62% of EDR (QA = Best) AOD retrievals fall within EE, and up to 46% of EDR AOD retrievals are significantly overestimated. At the temporal scale, despite some exceptions, both EDR and DB display a worse performance in summer for all statistics, which is likely related to larger cloud cover and higher relative humidity in the rainy season.

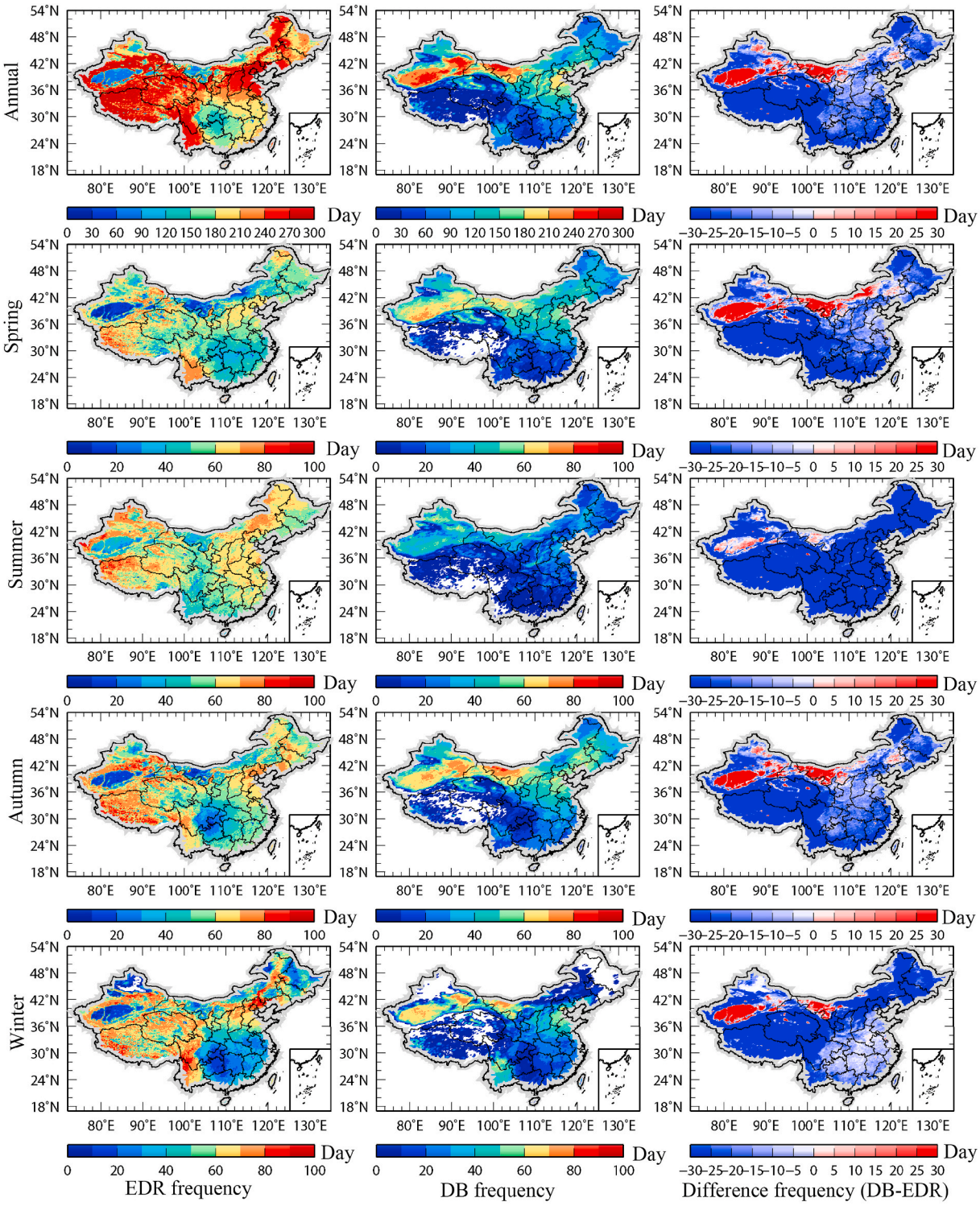

Fig. 14. Spatial frequencies of VIIRS EDR (left), DB (middle) AOD products and their differences (right) from 2013 to 2018 in China.

Uncertainty analyses reveal that both EDR and DB algorithms are impacted by surface properties and atmospheric conditions. In terms of surface characteristics, DB is less sensitive to NDVI under different aerosol loadings, while the EDR AOD bias becomes lower with the increase of NDVI. EDR performs well in dark surfaces but poorly in urban. By contrast, DB shows satisfactory performance in most land-use types, especially in urban. Furthermore, DB performs well in all landform types, while EDR only performs well in mountainous areas, with sufficient vegetation coverage. Furthermore, EDR shows the worst accuracy in coarse-mode-aerosol-dominated conditions; however, DB shows superior ability under diverse atmospheric conditions. Moreover, MODIS DT and DB algorithms show similar performances with VIIRS EDR and DB products in China due to the common algorithmic heritage. However, the VIIRS DB product shows the highest accuracy over both dark and bright surfaces, with almost all the best statistical metrics.

Spatiotemporal analyses suggest that the VIIRS DB products have a better ability to capture heavy dust events than EDR products. However, except for Northwest China, EDR has a higher AOD retrieval frequency

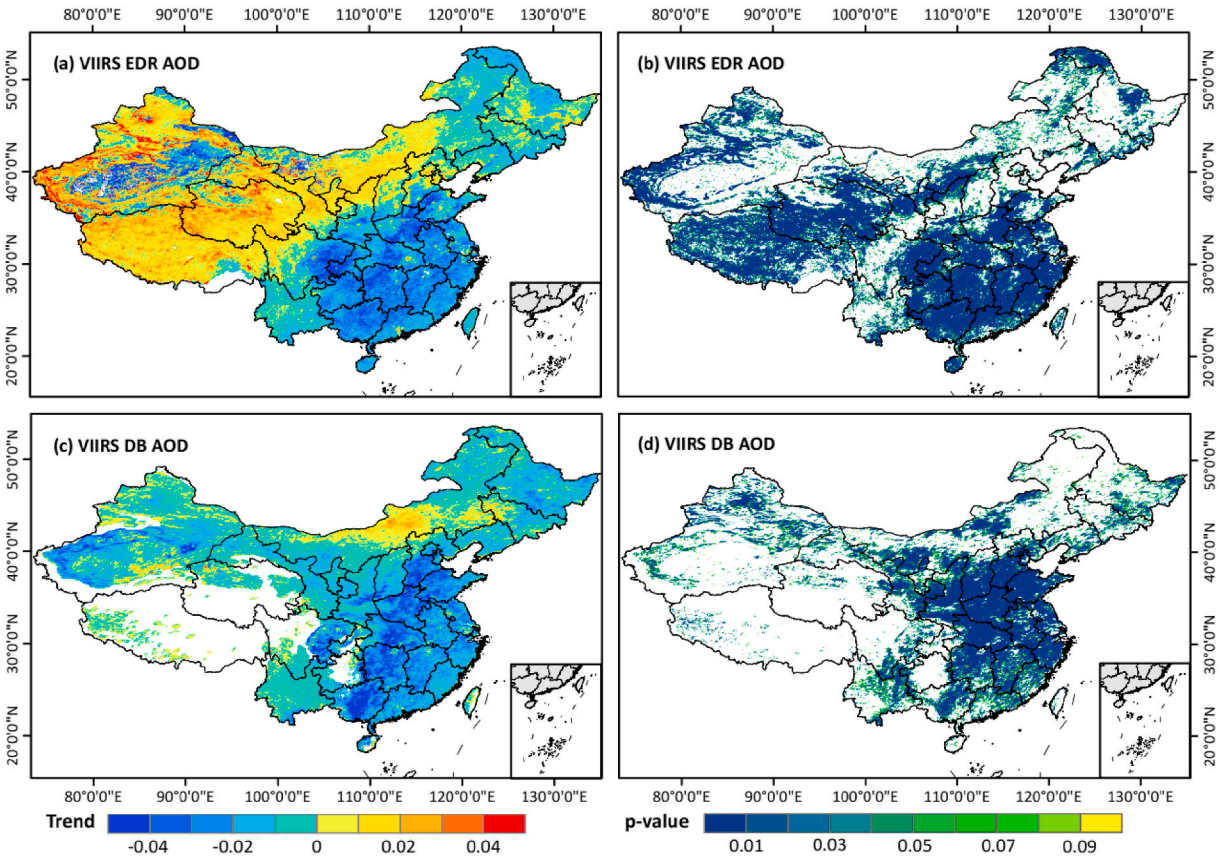

Fig. 15. Spatial distributions of linear trend (AOD yr^{-1}) calculated from deseasonalized VIIRS EDR (a) and DB (c) monthly AOD anomalies from 2013 to 2018 in China. (b) and (d) represent their corresponding significance level via p-value.

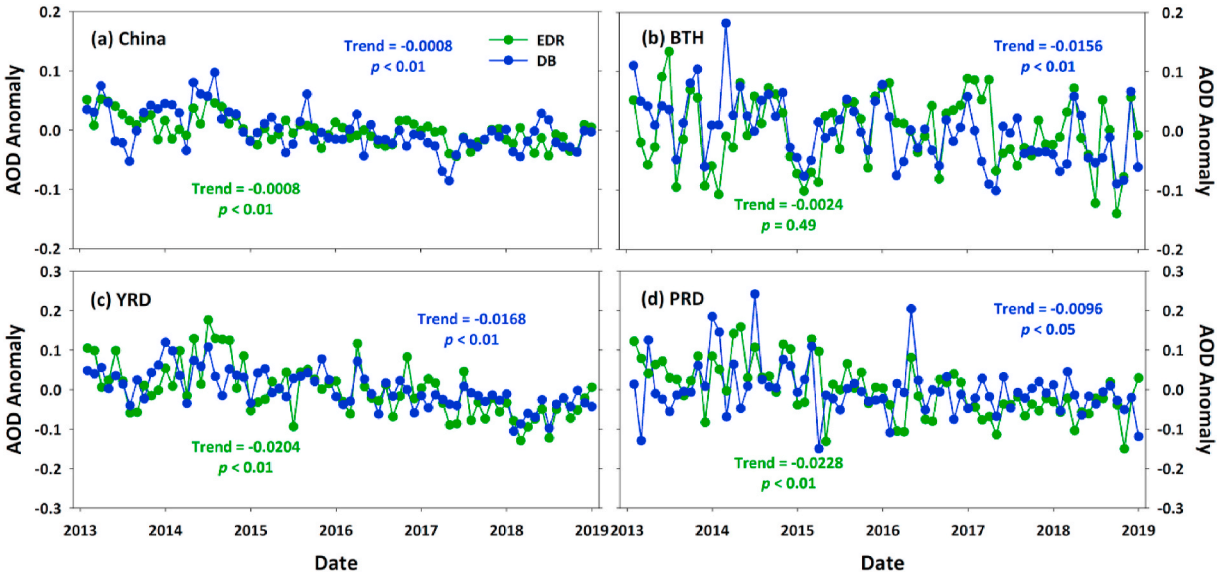

Fig. 16. Time series of deseasonalized monthly VIIRS EDR and DB AOD anomalies from 2013 to 2018 in China and each region.

than DB in most areas of China. EDR is characterized by higher AOD loadings than DB in Eastern and Southern China with rapid urbanization and industrialization. Both EDR and DB products can capture the same significant downward AOD trends in China, YRD, and PRD regions from 2013 to 2018, which benefits from the prevention and control of air pollution in China. However, opposite trends are observed in the BTH region and compared with the ground observations, and we find that DB products can capture the long-term aerosol change more accurately than EDR in China. In general, our study demonstrates that the VIIRS DB products show superior retrieval accuracy compared to EDR products, and it allows us to extend long-term aerosol records combined with MODIS products, which opens up new perspectives for future aerosol-related studies in China.

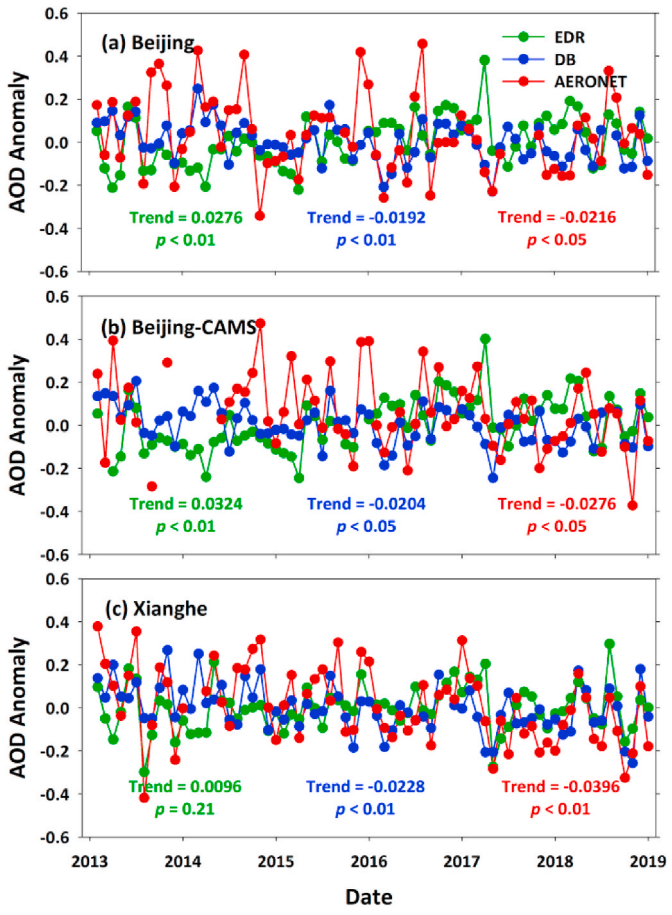

Fig. 17. Time series of deseasonalized monthly anomalies of VIIRS EDR (green), DB (blue), and AERONET (red) AOD measurements from 2013 to 2018 at Beijing (a), Beijing-CAMS (b), and Xianghe (c) sites. (For interpretation of the references to color in this figure legend, the reader is referred to the Web version of this article.)

Data availability

The VIIRS and MODIS series products are available from the NASA Earth Data (https://search.earthdata.nasa.gov/search), and AERONET ground measurements are available from NASA Goddard Space Flight Center (https://aeronet.gsfc.nasa). All data can be obtained by contacting the corresponding authors.

Author contribution

JW designed the research, and LH wrote the initial draft of this paper. LW, LS, and DL helped review and edit the paper. LZ, DJ, LL, RY, and ZZ helped collect and process the data. All authors made substantial contributions to this work.

Declaration of competing interest

The authors declare that they have no known competing financial interests or personal relationships that could have appeared to influence the work reported in this paper.

Acknowledgments

This study was supported by the National Key R&D Program of China (2017YFC1501702), and the National Natural Science Foundation of China (41975044, 41871019, and 41672355).

Appendix A. Supplementary data

Supplementary data to this article can be found online at https://doi.org/10.1016/j.atmosenv.2021.118265.

References

Cao, C., Xiong, J., Blonski, S., Liu, Q., Uprety, S., Shao, X., Bai, Y., Weng, F., 2013. Suomi NPP VIIRS sensor data record verification, validation, and long-term performance monitoring. J. Geophys. Res. Atmos. 118, 11–664.

Che, H., Zhang, X.Y., Xia, X., Goloub, P., Holben, B., Zhao, H., Wang, Y., Zhang, X.C., Wang, H., Blarel, L., Damiri, B., 2015. Ground-based aerosol climatology of China: aerosol optical depths from the China Aerosol Remote Sensing Network (CARSNET) 2002–2013. Atmos. Chem. Phys. 15, 7619–7652.

DeLuccia, F., Cao, C., Xiong, X., Wolfe, R., Oudrari, H., Chiang, K., Johnson, E., Mills, S., Liao, L., Moyer, D., Rausch, K., 2012. Suomi National Polar-Orbiting Partnership (NPP) Visible Infrared Imager Radiometer Suite (VIIRS) Sensor Data Record (SDR) Quality. Geoscience and Remote SensingSymposium. IGARSS.

Giles, D.M., Sinyuk, A., Sorokin, M.G., Schafer, J.S., Smirnov, A., Slutsker, I., Welton, E. J., 2019. Advancements in the Aerosol Robotic Network (AERONET) Version 3 database–automated near-real-time quality control algorithm with improved cloud screening for Sun photometer aerosol optical depth (AOD) measurements. Atmos. Meas. Tech. 12, 169–209.

Gupta, P., Levy, R.C., Mattoo, S., Remer, L.A., Munchak, L.A., 2016. A surface reflectance scheme for retrieving aerosol optical depth over urban surfaces in MODIS Dark Target retrieval algorithm. Atmos. Meas. Tech. 9, 3293–3308.

He, L., Wang, L., Lin, A., Zhang, M., Bilal, M., Tao, M., 2017. Aerosol optical properties and associated direct radiative forcing over the Yangtze River Basin during 2001–2015. Rem. Sens. 9, 746. https://doi.org/10.3390/rs9070746.

He, L., Wang, L., Lin, A., Zhang, M., Bilal, M., Wei, J., 2018. Performance of the NPP-VIIRS and aqua-MODIS aerosol optical depth products over the Yangtze River basin. Rem. Sens. 10, 117. https://doi.org/10.3390/rs10010117.

He, L., Wang, L., Huang, B., Wei, J., Zhou, Z., Zhong, Y., 2020. Anthropogenic and meteorological drivers of 1980–2016 trend in aerosol optical and radiative properties over the Yangtze River Basin. Atmos. Environ. 223, 117188 https://doi.org/10.1016/j.atmosenv.2019.117188.

Holben, B.N., Eck, T.F., Slutsker, I.A., Tanre, D., Buis, J.P., Setzer, A., Lavenu, F., 1998. AERONET—a federated instrument network and data archive for aerosol characterization. Remote Sens. Environ. 66, 1–16.

Hsu, N.C., Tsay, S.C., King, M.D., Herman, J.R., 2006. Deep Blue retrievals of Asian aerosol properties during ACE-Asia. IEEE T. Geosci. Remote. 44, 3180–3195.

Hsu, N.C., Jeong, M.J., Bettenhausen, C., Sayer, A.M., Hansell, R., Seftor, C.S., Tsay, S.C., 2013. Enhanced Deep Blue aerosol retrieval algorithm: the second generation. J. Geophys. Res. Atmos. 118, 9296–9315.

Hsu, N.C., Lee, J., Sayer, A.M., Kim, W., Bettenhausen, C., Tsay, S.C., 2019. VIIRS Deep Blue aerosol products over land: extending the EOS long-term aerosol data records. J. Geophys. Res. Atmos. 124, 4026–4053.

Huang, J., Kondragunta, S., Laszlo, I., Liu, H., Remer, L.A., Zhang, H., Petrenko, M., 2016. Validation and expected error estimation of Suomi-NPP VIIRS aerosol optical thickness and Ångström exponent with AERONET. J. Geophys. Res. Atmos. 121, 7139–7160.

Huang, J., Minnis, P., Yi, Y., Tang, Q., Wang, X., Hu, Y., Winker, D., 2007. Summer dust aerosols detected from CALIPSO over the Tibetan Plateau. Geophys. Res. Lett. 34 https://doi.org/10.1029/2007GL029938.

Jackson, J.M., Liu, H., Laszlo, I., Kondragunta, S., Remer, L.A., Huang, J., 2013. Suomi-NPP VIIRS aerosol algorithms and data products. J. Geophys. Res. Atmos. 118 (22), 12673–12689.

Leeuw, G.D., Sogacheva, L., Rodriguez, E., Kourtidis, K., Georgoulias, A.K., Alexandri, G., Xue, Y., 2018. Two decades of satellite observations of AOD over mainland China using ATSR-2, AATSR and MODIS/Terra: data set evaluation and large-scale patterns. Atmos. Chem. Phys. 18, 1573–1592.

Levy, R.C., Mattoo, S., Munchak, L.A., Remer, L.A., Sayer, A.M., Patadia, F., Hsu, N.C., 2013. The Collection 6 MODIS aerosol products over land and ocean. Atmos. Meas. Tech. 6, 2989. https://doi.org/10.5194/amt-6-2989-2013.

Li, Z.Q., Xu, H., Li, K.T., Li, D.H., Xie, Y.S., Li, L., Deng, R.R., 2018. Comprehensive study of optical, physical, chemical, and radiative properties of total columnar atmospheric aerosols over China: an overview of Sun–Sky Radiometer Observation Network (SONET) measurements. Bull. Am. Meteorol. Soc. 99, 739–755.

Liu, H., Remer, L.A., Huang, J., Huang, H.C., Kondragunta, S., Laszlo, I., Jackson, J.M., 2014. Preliminary evaluation of S-NPP VIIRS aerosol optical thickness. J. Geophys. Res. Atmos. 119, 3942–3962.

Liu, N., Zou, B., Feng, H., Wang, W., Tang, Y., Liang, Y., 2019. Evaluation and comparison of multiangle implementation of the atmospheric correction algorithm, Dark Target, and Deep Blue aerosol products over China. Atmos. Chem. Phys. 19, 8243–8268.

Martins, V.S., Lyapustin, A., de Carvalho, L.A.S., Barbosa, C.C.F., Novo, E.M.L.M., 2017. Validation of high-resolution MAIAC aerosol product over South America. J. Geophys. Res. Atmos. 122, 7537–7559.

Mei, L., Zhao, C., de Leeuw, G., Burrows, J.P., Rozanov, V., Che, H.Z., 2019a. A critical evaluation of Deep Blue algorithm derived AVHRR aerosol product over China. J. Geophys. Res. Atmos. 124 https://doi.org/10.1029/2018JD029929.

Mei, L., Zhao, C.X., de Leeuw, G., Rozanov, V., Che, H.Z., Vountas, M., Burrows, J.P., 2019b. Understanding MODIS Dark-Target collection 5 and 6 aerosol data over

China: effect of surface type, aerosol loading and aerosol absorption. Atmos. Res. 228, 161–175.
Mhawish, A., Banerjee, T., Sorek-Hamer, M., Lyapustin, A., Broday, D.M., Chatfield, R., 2019. Comparison and evaluation of MODIS multi-angle implementation of atmospheric correction (MAIAC) aerosol product over south asia. Remote Sens. Environ. 224, 12–28.
Popp, T., de Leeuw, G., Bingen, C., Brühl, C., Capelle, V., Chedin, A., Clarisse, L., Dubovik, O., Grainger, R., Griesfeller, J., Heckel, A., Kinne, S., Klüser, L., Kosmale, M., Kolmonen, P., Lelli, L., Litvinov, P., Mei, L., North, P., Pinnock, S., Povey, A., Robert, C., Schulz, M., Sogacheva, L., Stebel, K., Zweers, D.S., Thomas, G., Tilstra, S., Vandenbussche, L.G., Veefkind, P., Vountas, M., Xue, Y., 2016. Development, production and evaluation of aerosol Climate Data Records from European satellite observations (Aerosol_cci). Rem. Sens. 8, 421. https://doi.org/10.3390/rs8050421.
Sayer, A.M., 2020. How long is too long? variogram analysis of aeronet data to aid aerosol validation and intercomparison studies. Earth Space Sci 7 (9). https://doi.org/10.1029/2020EA001290.
Sayer, A.M., Hsu, N.C., Lee, J., Bettenhausen, C., Kim, W.V., Smirnov, A., 2018. Satellite Ocean aerosol retrieval (SOAR) algorithm extension to S-NPP VIIRS as part of the "deep blue" aerosol project. J. Geophys. Res. Atmos. 123, 380–400.
Sayer, A.M., Hsu, N.C., Lee, J., Kim, W.V., Dutcher, S.T., 2019. Validation, stability, and consistency of MODIS Collection 6.1 and VIIRS Version 1 Deep Blue aerosol data over land. J. Geophys. Res. Atmos. 124, 4658–4688.
Sayer, A.M., Munchak, L.A., Hsu, N.C., Levy, R.C., Bettenhausen, C., Jeong, M.J., 2014. MODIS Collection 6 aerosol products: comparison between Aqua's e-Deep Blue, Dark Target, and "merged" data sets, and usage recommendations. J. Geophys. Res. Atmos. 119, 13–965.
Sundström, A.M., Arola, A., Kolmonen, P., Xue, Y., de Leeuw, G., Kulmala, M., 2015. On the use of satellite remote sensing-based approach for determining aerosol direct radiative effect over land: a case study over China. Atmos. Chem. Phys. 15, 505–518.
Wei, J., Sun, L., Huang, B., Bilal, M., Zhang, Z., Wang, L., 2018. Verification, improvement and application of aerosol optical depths in China Part 1: inter-comparison of NPP-VIIRS and Aqua-MODIS. Atmos. Environ. 175, 221–233.
Wei, J., Li, Z., Sun, L., Peng, Y., Liu, L., He, L., Qin, W., Cribb, M., 2020. MODIS Collection 6.1 3 km resolution aerosol optical depth product: global evaluation and uncertainty analysis. Atmos. Environ. 240, 117768 https://doi.org/10.1016/j.atmosenv.2020.117768.
Wei, J., Li, Z., Guo, J., Sun, L., Huang, W., Xue, W., Fan, T., Cribb, M., 2019a. Satellite-derived 1-km-resolution PM_1 concentrations from 2014 to 2018 across China. Environ. Sci. Technol. 53 (22), 13265–13274.
Wei, J., Li, Z., Lyapustin, A., Sun, L., Peng, Y., Xue, W., Su, T., Cribb, M., 2021a. Reconstructing 1-km-resolution high-quality $PM_{2.5}$ data records from 2000 to 2018 in China: spatiotemporal variations and policy implications. Remote Sens. Environ. 252, 112136 https://doi.org/10.1016/j.rse.2020.112136.
Wei, J., Li, Z., Peng, Y., Sun, L., 2019a. MODIS Collection 6.1 aerosol optical depth products over land and ocean: validation and comparison. Atmos. Environ. 201, 428–440.
Wei, J., Li, Z., Sun, L., Yang, Y., Zhao, C., Cai, Z., 2019b. Enhanced aerosol estimations from Suomi-NPP VIIRS images over heterogeneous surfaces. IEEE T. Geosci. Remote. 57, 9534–9543.
Wei, J., Li, Z., Xue, W., Sun, L., Fan, T., Liu, L., Su, T., Cribb, M., 2021b. The ChinaHighPM_{10} dataset: generation, validation, and spatiotemporal variations from 2015 to 2019 across China. Environment International 146, 106290. https://doi.org/10.1016/j.envint.2020.106290.
Wei, J., Peng, Y., Mahmood, R., Sun, L., Guo, J., 2019c. Intercomparison in spatial distributions and temporal trends derived from multi-source satellite aerosol products. Atmos. Chem. Phys. 19, 7183–7207.
Xia, X., Che, H., Zhu, J., Chen, H., Cong, Z., Deng, X., Liu, Q., 2016. Ground-based remote sensing of aerosol climatology in China: aerosol optical properties, direct radiative effect and its parameterization. Atmos. Environ. 124, 243–251.
Xiao, Q., Zhang, H., Choi, M., Li, S., Kondragunta, S., Kim, J., Liu, Y., 2016. Evaluation of VIIRS, GOCI, and MODIS Collection 6 AOD retrievals against ground sun photometer observations over East Asia. Atmos. Chem. Phys. 16, 1255–1269.
Xu, C., Ma, Y.M., Panday, A., Cong, Z.Y., Yang, K., Zhu, Z.K., Zhao, L., 2014. Similarities and differences of aerosol optical properties between southern and northern sides of the Himalayas. Atmos. Chem. Phys. 14 (6), 3133–3149.
Zhang, J., Reid, J.S., Alfaro-Contreras, R., Xian, P., 2017. Has China been exporting less particulate air pollution over the past decade? Geophys. Res. Lett. 44, 2941–2948.
Zhu, J., Xia, X., Wang, J., Che, H., Chen, H., Zhang, J., Ayoub, M., 2017. Evaluation of aerosol optical depth and aerosol models from VIIRS retrieval algorithms over North China Plain. Rem. Sens. 9, 432. https://doi.org/10.3390/rs9050432.